

CR-61676

13

MCR-68-11 Copy No.

**Design, Fabrication, and Testing
of Subscale Propellant Tanks
with Capillary Traps**

Final Report

GPO PRICE \$ _____

CFSTI PRICE(S) \$ _____

Hard copy (HC) 3.00

Microfiche (MF) _____

ff 653 July 65

March 1968

Under Contract with:

National Aeronautics and Space Administration
George C. Marshall Space Flight Center
Contract No. NAS8-20837
Huntsville, Alabama

MARTIN MARIETTA CORPORATION



FACILITY FORM 602

N68-19836

(ACCESSION NUMBER)

(THRU)

50
(PAGES)

1
(CODE)

NASA-CR-61675
(NASA CR OR TMX OR AD NUMBER)

32
(CATEGORY)

MCR-68-11

DESIGN, FABRICATION AND TESTING OF SUBSCALE
PROPELLANT TANKS WITH CAPILLARY TRAPS


Report Period: 6/26/67 to 3/15/68

March 1968

Prepared By:

Thomas R. Barksdale
Howard L. Paynter

Approved By:


Howard L. Paynter

Contract NAS8-20837
Contract Control No. 1-7-56-20157

Martin-Marietta Corporation
Denver Division
Denver, Colorado

FOREWORD

This report was prepared by Martin-Marietta Corporation, Denver Division, Denver, Colorado, under Contract NAS8-20837, Design, Fabrication and Testing of Subscale Propellant Tanks With Capillary Traps, for the George C. Marshall Space Flight Center of the National Aeronautics and Space Administration. The work was administered under the technical direction of Mr. Leon J. Hastings of the Propulsion and Vehicle Engineering Laboratory of the George C. Marshall Space Flight Center.

TABLE OF CONTENTS

	<u>Page No.</u>
Foreword	i
Table of Contents	ii
List of Figures	iii
List of Tables	iii
Summary	iv
Nomenclature	iv
I. Introduction	1
II. Experimental Apparatus and Procedure	4
A. Drop Tower	4
B. Test Specimens	6
C. Test Liquids	7
D. Procedure	13
III. Experimental Results	14
IV. Discussion of Results	22
V. Conclusions and Recommendations	31
A. Conclusions	31
B. Recommendations	31
VI. References	35
Distribution	38
Appendix A: Literature Review	39

LIST OF FIGURES

<u>No.</u>	<u>Description</u>	<u>Page</u>
1	Wetting Liquid in a Cylindrical Tube.	2
2	Martin-Marietta Low-g Drop Tower.	4
3	Low-g Capsule Assembly.	5
4	Inner-Capsule (Test Cell).	6
5	Cylindrical Test Specimens.	6
6	Camera Test Setup.	6
7	Perforated Plates #7 and #8.	8
8	Perforated Plates #12 and #14.	8
9	Perforated Plate #16.	8
10	Perforated Plate #13.	8
11	Typical Screen Barriers.	9
12	Typical Hole Pattern For Plates With Constant Hole Sizes.	9
13	Stability Characteristics of Perforated Plate Barriers.	19
14	Stability Characteristics of Square Weave Screen.	20
15	Pore Stability (Run No. 8a) and Instability (Run No. 2a).	21
16	Filmed Sequence of Run No. 2.	23
17	Filmed Sequence of Run No. 22a.	24
18	Filmed Sequence of Run No. 23a.	25
19	Gas Ingestion Phenomena (Run No. 31d).	29
20	Compartmented Tank with Perforated Partitions.	31
21	Compartmented Tank with Baffle-like Partitions.	32
22	Proposed Orbital Experiment.	34

LIST OF TABLES

<u>No.</u>	<u>Description</u>	<u>Page</u>
I	Foraminous Barrier Specifications	10
II	Physical Properties - Test Liquids and Storable Propellants	12
III	Summary of Test Results	16
IV	Pertinent Variables and Their Uncertainty Intervals	27
V	Apollo Applications Program Launch Schedule	33

SUMMARY

An experimental study was conducted in Martin-Marietta's drop tower to determine the hydrostatic stability characteristics of perforated plates and square-weave screens. Tests were made over a controllable and repeatable acceleration range from 0.0013- to 0.055-g during the 2.1-sec drop interval using test liquids that simulated storable liquid propellants. The acceleration was applied normal to the flat, foraminous barriers tending to resettle liquid from beneath the barriers to the opposite end of the cylindrical tanks. Test results for the bare (uncoated) plates and screens verified that the Bo number, a dimensionless ratio of acceleration-to-capillary forces, is the criterion for predicting hydrostatic stability of the liquid-gas interface. The critical Bo number, delineating the stable and unstable regions, was verified for the plates with circular holes to be 0.84 based on pore radius. Test data for the screens tend to support a critical Bo number value of 0.45 based on one-half of the open width of the square weave screen.

The pore stability data are directly applicable to the design of passive, capillary systems that control liquid propellant during the coast phases of space missions.

NOMENCLATURE

<u>Symbol</u>	<u>Denotation</u>
a	Acceleration
Bo	Bond number
σ	Kinematic surface tension
C	Carbon tetrachloride
d	Diameter
F	Freon TF
f	Force
g	Gravitational acceleration
GN ₂	Gaseous nitrogen
M	Methanol
m	Mass
N	Number of holes
P	Pressure
Δp	Differential pressure
ρ	Mass density
$\Delta \rho$	Mass density difference (liquid minus vapor)
R	Radius
Δt	Low-g test duration
T	Thickness
W	Weight
We	Weber number
w	Uncertainty interval
z	Liquid height
σ	Liquid-vapor surface tension
θ	Liquid-to-solid contact angle

<u>Subscripts</u>	<u>Denotation</u>
B	Bubble
Bo	Bond number
c	Critical
f	Force
l	liquid
m	Mass
P	Pressure
R	Radius
ρ	Mass density

I. INTRODUCTION

The use of foraminous material, screen or perforated plate, to control fluids during low-g operation has been under investigation during the past few years, Refs. 1 thru 16. The foraminous material is configured within the storage tank to properly orient and separate the two fluid phases, liquid and vapor (ullage). The ullage pressure and interfacial surface tension control and maintain separation of the fluid phases, Ref. 13. This is one of the more attractive features of capillary systems. They are entirely passive and require no additional power or external energy source to provide:

- a) restart of liquid rocket engines;
- b) control of liquid motion (slosh);
- c) fluid center-of-mass control;
- d) elimination of suction dip (liquid draining phenomenon);
- e) transfer and resupply of liquids; and
- f) venting of vapor.

The basic operational principle of these systems is that ullage pressure supports the liquid in its desired location while surface tension stabilizes the liquid-ullage interface at the foraminous material. One may quickly check this principle in a simple bench test by taking open-ended, cylindrical tubes of different diameters, 1/8 to 1-in., and immersing one end of each tube in a wetting liquid, such as methanol*, and then withdrawing the tube. It is found that liquid will stay in the smaller tubes ($d < 1/4$ -in.) only when the open-end not immersed is capped off. (If the tubes are not capped, liquid is lost regardless of size.) For the larger tubes ($d > 1/4$ -in.), liquid is lost even with the tubes capped. This phenomenon is explainable using Figure 1. The wetting liquid (meniscus downward) is pictured in the tube after lifting it from the liquid reservoir. Surface tension and gravitational acceleration tend to displace liquid from the tube. Surface tension does not support the liquid. The supporting force is provided by the difference in pressure at the top and bottom of the liquid column. This supporting pressure effect is readily seen by uncapping the smaller tubes. The pressure difference, $P_0 - P_1$, becomes zero and liquid is lost. If one is able to cap the tube with no ullage above the liquid column, liquid can

*Liquids of interest for space applications are considered wetting, i.e., they possess a liquid-to-solid contact angle, θ , less than ninety degrees when in contact with metals. As seen in Table II, page 12, the liquid storable propellants are extremely good wetters, i.e., $\theta \approx 0^\circ$. If one uses glass tubes in the capillary demonstration it is best then to use a liquid like methanol, instead of water, to simulate the storable propellants and cryogenics. Water tends to be non-wetting to glass, (Private communication: W. J. Masica, NASA LeRC, and H. L. Paynter, MMC, 19 July 1967).

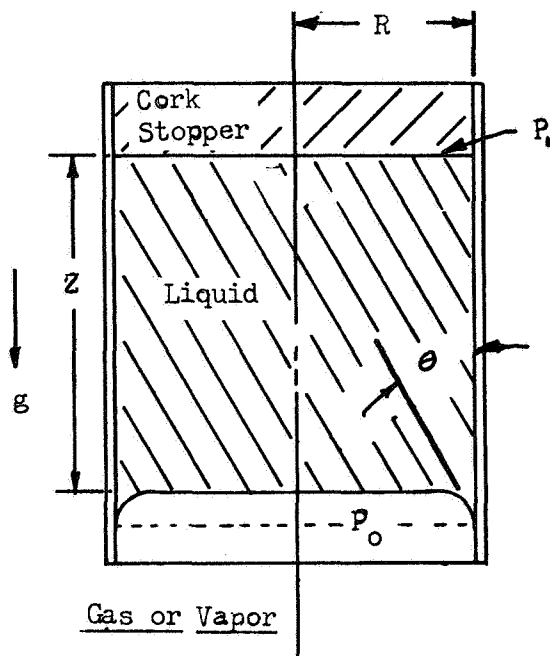


Fig. 1. Wetting Liquid in a Cylindrical Tube

only be lost by pulling a vacuum at the top of the liquid column. This zero ullage condition provides the maximum supporting pressure difference, $P_0 - P_v$ (P_1 is now vapor pressure). If, however, the tube is capped with an initial ullage volume that provides no pressure support ($P_0 = P_1$), liquid is lost until a pressure difference is reached that will support the weight of the liquid. The liquid weight is:

$$W_L = \rho_L Z \pi R^2 g \quad (1)$$

while the supporting pressure force is;

$$F_p = (P_0 - P_1) \pi R^2. \quad (2)$$

It is evident from equations 1 and 2 that for a given supporting pressure difference a liquid height is supported regardless of tube radius. The simple experiments will verify this up to a maximum tube size, about 1/4-in. dia. for methanol. Beyond this critical size*, the liquid-gas interface at the free surface of the liquid (bottom of the tube) becomes unstable, air enters, and liquid is lost. Surface tension tends to stabilize the interface, Figure 1. As a result, the free surface can be stabilized past the critical tube diameter by reducing the effective open-end area. One way to do this is to place a screen or perforated plate at the bottom of the tube. This is the basic technique used in the design of capillary systems.

Several investigators have studied the interfacial stabilizing effect provided by perforated plates (Ref. 17) and screens (Refs. 17 and 18) under Earth's gravity (one-g). The standard approach employed is to measure the hydrostatic head at which the pore becomes

*W. J. Masica, et al, Ref. 19, verified experimentally that this critical tube radius is predictable from the following relationship:

$$R_c = 0.92 \left[\frac{\sigma}{\Delta \rho a} \right]^{1/2}. \quad \text{The Bond number criterion for stability (based on radius) obtained from the NASA LeRC data and valid for } \theta = 0^\circ \text{ is } Bo = 0.84.$$

unstable. Of the several techniques, the bubble point method is the most widely used and accepted. The foraminous material is covered by a thin layer ($\frac{1}{2}$ -in., or less) of liquid, usually isopropyl alcohol, and its underside is pressurized slowly with air or gaseous nitrogen. The pressure at which the first bubble passes through the material is termed the bubble point (gas pressure retention capability).

Hydrostatic pore stability tests under one-g are limited, however, to relatively small pore openings (0.02-in., or less) since a measurable head or pressure is required.

The purpose of this experimental program was to investigate hydrostatic stability for larger pore sizes ($d \geq 0.02$ -in.) in the MMC drop tower under accelerations ranging from 0.001- to 0.05-g (acceleration vector normal to the flat foraminous material). Perforated plates and square-weave screens were to be investigated in cylindrical tanks using test liquids that simulated a wide range of storable propellants. The program's technical objectives were (1) verification of the Bo number criterion, (2) verification of the functional relation of the liquid properties, and pore size and configuration, involved in the criterion, and (3) to establish the numerical value of the critical Bo at which instability of the liquid-gas interface occurs.

The report describes the experimental apparatus and test procedure in Chapter II. The experimental results and a discussion of results are presented in Chapters III and IV, respectively. Conclusions and recommendations are included in Chapter V, followed by a bibliography in Chapter VI. A review of the literature pertaining to hydrostatic pore stability is presented in Appendix A as background material for this experimental study.

II. EXPERIMENTAL APPARATUS AND PROCEDURE

A. Drop Tower

The experimental program was conducted in the Martin-Marietta drop tower located at Denver. The drop tower, Figure 2, provides a usable low-g test time of 2.1-sec. The drop system uses a two capsule assembly, Figure 3, consisting of an outer capsule, or drag shield, and an inner capsule which contains the experiment, power supply, and desired instrumentation, Figure 4. Inner capsule constant acceleration levels of 0.001-, 0.02-, and 0.05-g (nominal) were provided for this program by a constant force supplied by NEG'ATOR* spring motors, Fig. 3. The force was applied in the same direction as the gravitational force for all tests. During each drop, the inner capsule was accelerated vertically downward within the drag shield, contacting the bottom of the drag shield just prior to termination of free-fall. Safe deceleration of the entire system is accomplished within 0.15-sec when the legs and annular ring assembly, attached to the bottom of the drag shield, embed themselves in wheat stored in a large, cylindrical bin.

Air drag on the inner capsule and any piston effect due to relative travel between the inner capsule and drag shield are reduced to an insignificant level ($<10^{-5}$ g) by evacuating the space between the two capsules. Absolute pressure levels of less than 5 mm Hg were provided for all tests.

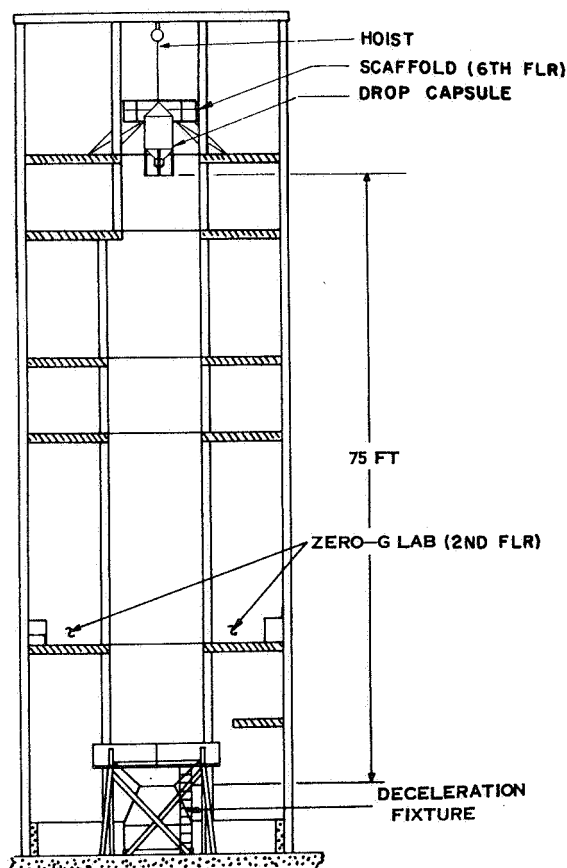


Figure 2: Martin-Marietta Low-g Drop Tower

The relative travel distance between capsule and drag shield required for a given acceleration is obtained by adjusting the length of the inner capsule suspension hook assembly and the aluminum bottoming tube, Figure 3. The tube also protects the inner capsule in the event the capsule does not bottom properly in the drag shield prior to drop termination. Impact energy is absorbed during crushing of the tube.

*Tradename. Hunter Spring Company, Hatfield, Pa.

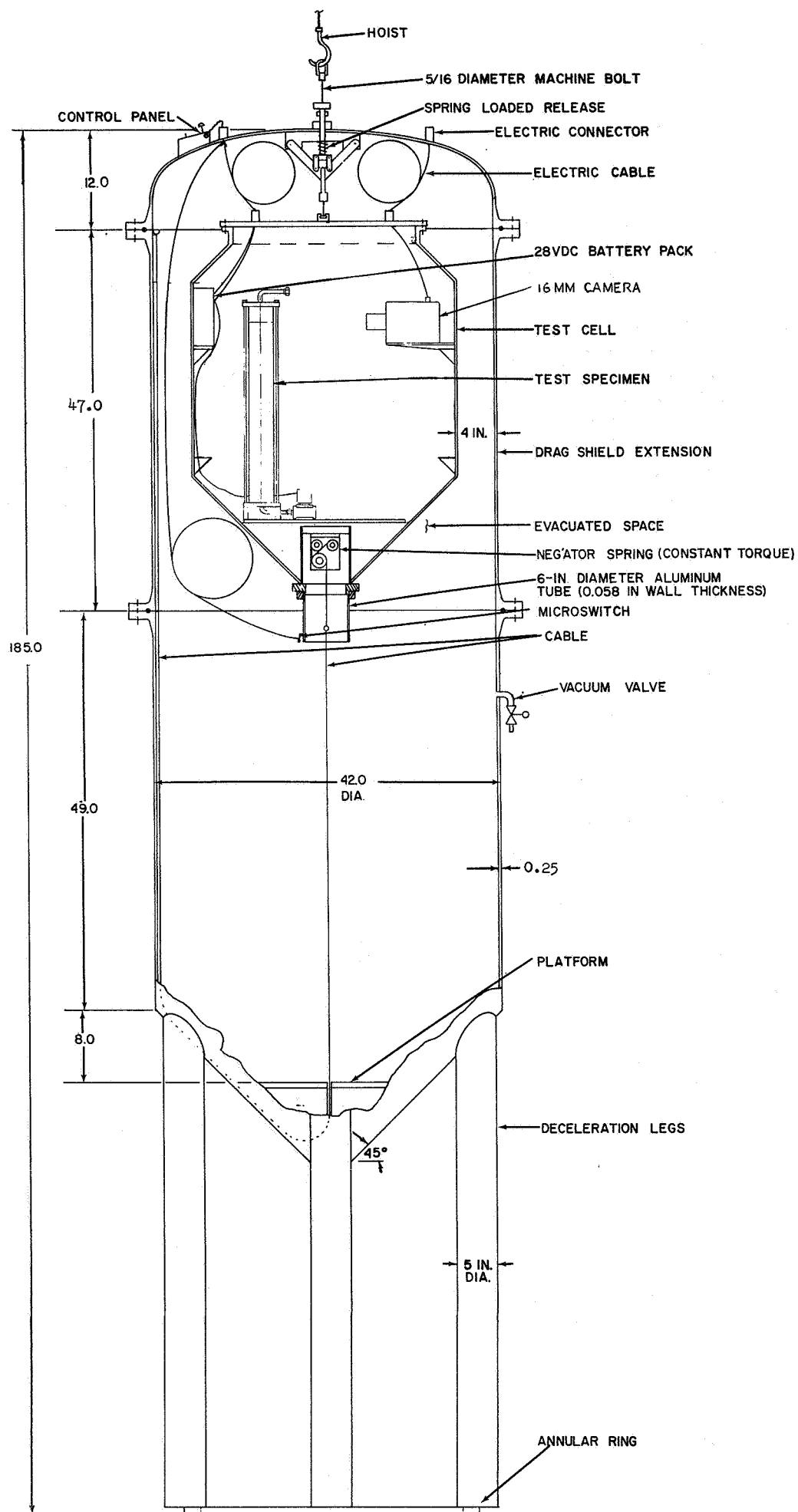


Figure 3. Low-g Capsule Assembly

B. Test Specimens

Two test specimens, Figures 4 and 5, were mounted on the inner capsule test platform in view of the 16 mm movie camera, Figure 6, for each drop. Each specimen consisted of two transparent cylinders, $5\frac{1}{2}$ -in. O.D., a perforated plate or square weave screen barrier, aluminum end plates and tie rods. The longer cylinder, 6-in., served as the bottom portion of the 10-in. specimen and was filled with liquid to provide a 6-in. hydrostatic head for the barrier during the test. The cylinder above the barrier was 4-in. long. For the initial tests, Plexiglas cylinders ($\frac{1}{4}$ -in. wall thickness) were used. Contrary to a pre-test material compatibility investigation, both Freon TF and carbon tetrachloride severely attacked the Plexiglas cylinders rendering them unfit after one test. The etching action on the inner-walls made the cylinders opaque. As a result, Pyrex glass cylinders were used during the remainder, and major portion of, the program. Flat gaskets made from rubber, Viton A*, and Dow Corning's Aerospace Sealant were used for seals between the cylinders and mating surfaces. The tie rods provided the compressive force to effect the seal.

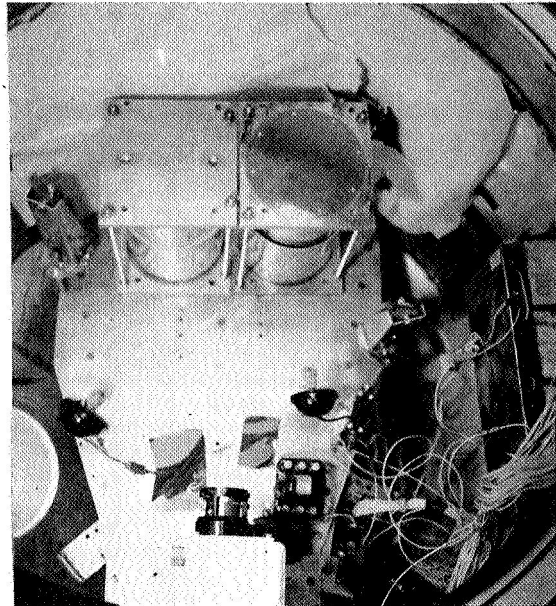


Figure 4: Inner capsule

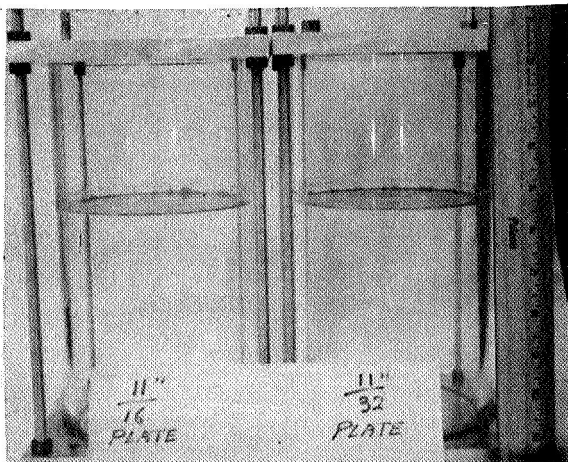


Figure 5: Cylindrical Test Specimens

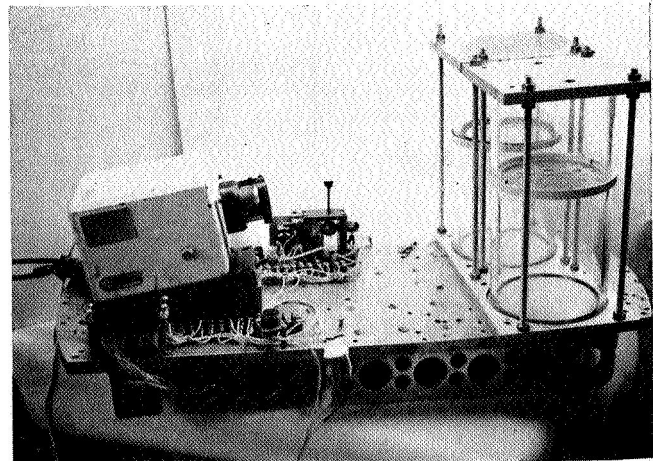


Figure 6: Camera Setup

A total of 52 barriers, 39 perforated plates and 13 square weave screens was used for the hydrostatic low-g tests. Pertinent dimensions of these barriers are presented in Table I. The first set of perforated plates was made from stainless steel. All other sets were made from aluminum. The latter material was preferred due to better machinability (closer hole tolerance). The holes (pores) in the plates were drilled and then reamed to the sizes listed in Table I. The square weave screen mesh sizes shown in the table are per the screen manufacturer.

Screen and plate barriers are pictured in Figures 7 thru 12 and are representative of the different hole patterns used in the program. These basic patterns and the dimensions presented in Table I depict the screen and plate specimens used in the program.

C. Test Liquids

Three liquids, methanol, carbon tetrachloride and Freon TF, were selected to simulate a wide range of storable propellants. The important physical properties for similitude in hydrostatic tests are kinematic surface tension, σ , and liquid-to-solid contact angle, θ . A comparison of the values for the test liquids and storable propellants is presented in Table II. It is seen that the σ range of the test liquids is adequate since it covers the oxidizers and extends into the fuels. It does not cover the monopropellants, however.

The storables are essentially totally-wetting ($\theta \approx 0^\circ$) to aluminum, titanium and stainless steel (Ref. 20), materials usually employed for propellant tankage. Since Plexiglas and Pyrex cylinders were used in the test program for visual observation, test liquids were selected with surface tensions less than $2.67 \times 10^{-3} \text{ lb}_f/\text{ft}$ to assure wettability with the cylinders, Ref. 21. (This was one of the reasons why the monopropellants were not simulated. Liquids such as water or water-methanol mixtures could cover the monopropellant σ range, however, their higher surface tensions would make them non-wetting to the cylinders.) Since the test liquids are wetting to the metallic foraminous specimens, the test specimens and test liquids simulated the wetting condition of a storable propellant in a metal storage tank.

A small trace of dye was added to the test liquids to provide better photographic quality. The dye did not affect the physical properties of the liquids.

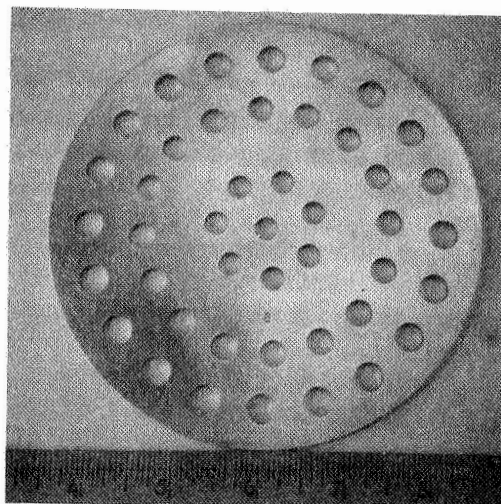
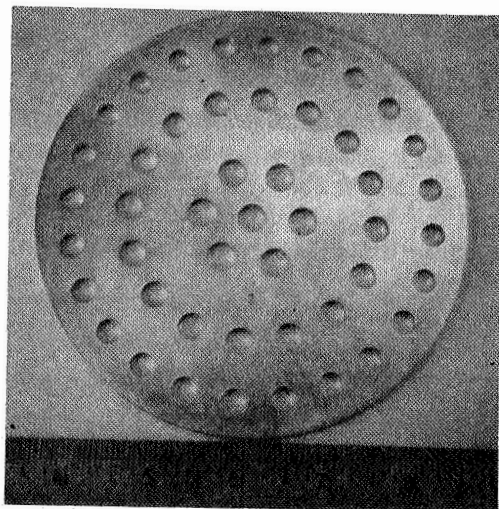


Figure 7: Plate #7 (left) and Plate #8 (right)

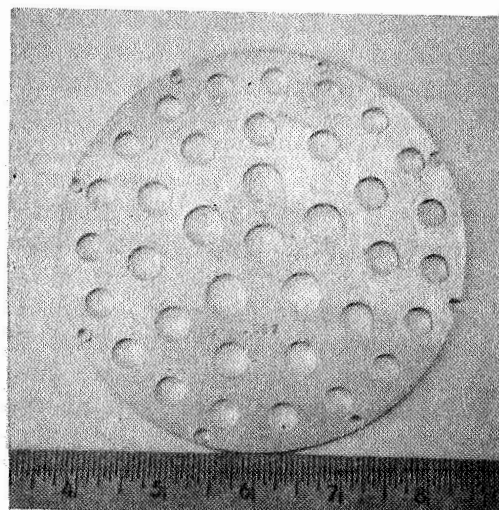
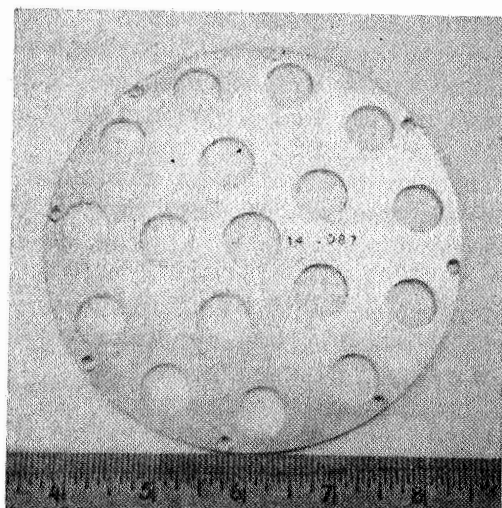


Figure 8: Plate #14 (left) and Plate #12 (right)

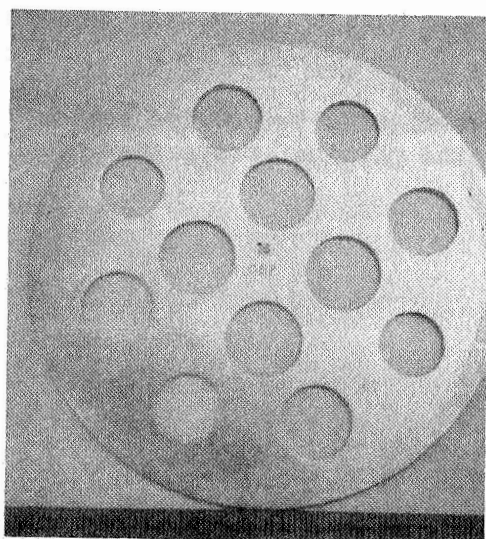


Figure 9: Plate #16

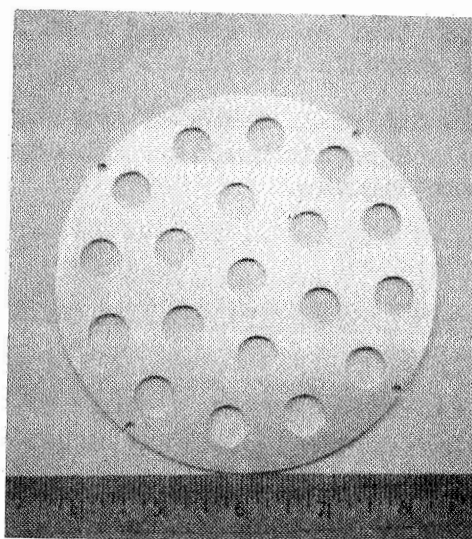
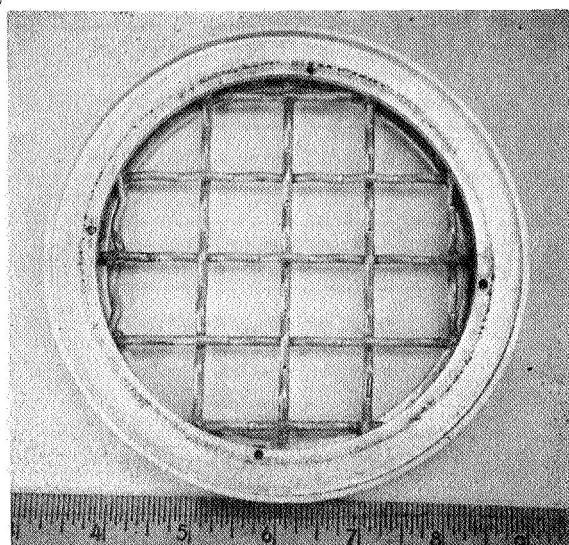
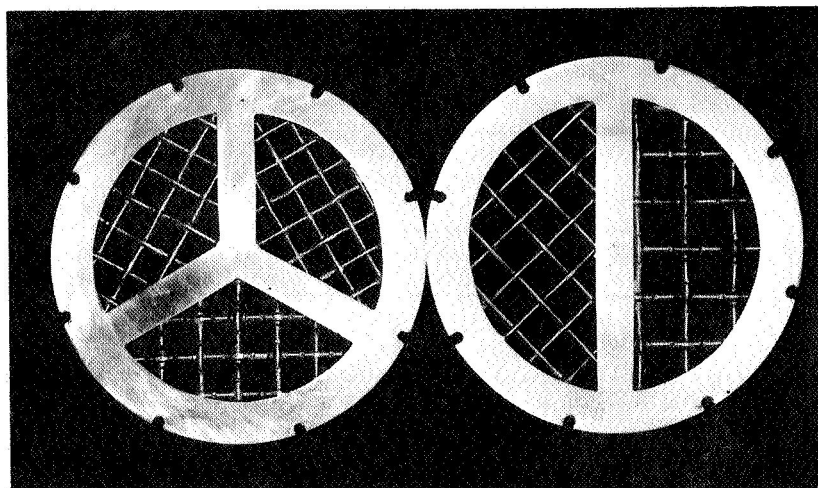


Figure 10: Plate #13



S-8



S-3

S-2

Figure 11: Typical Screen Barriers

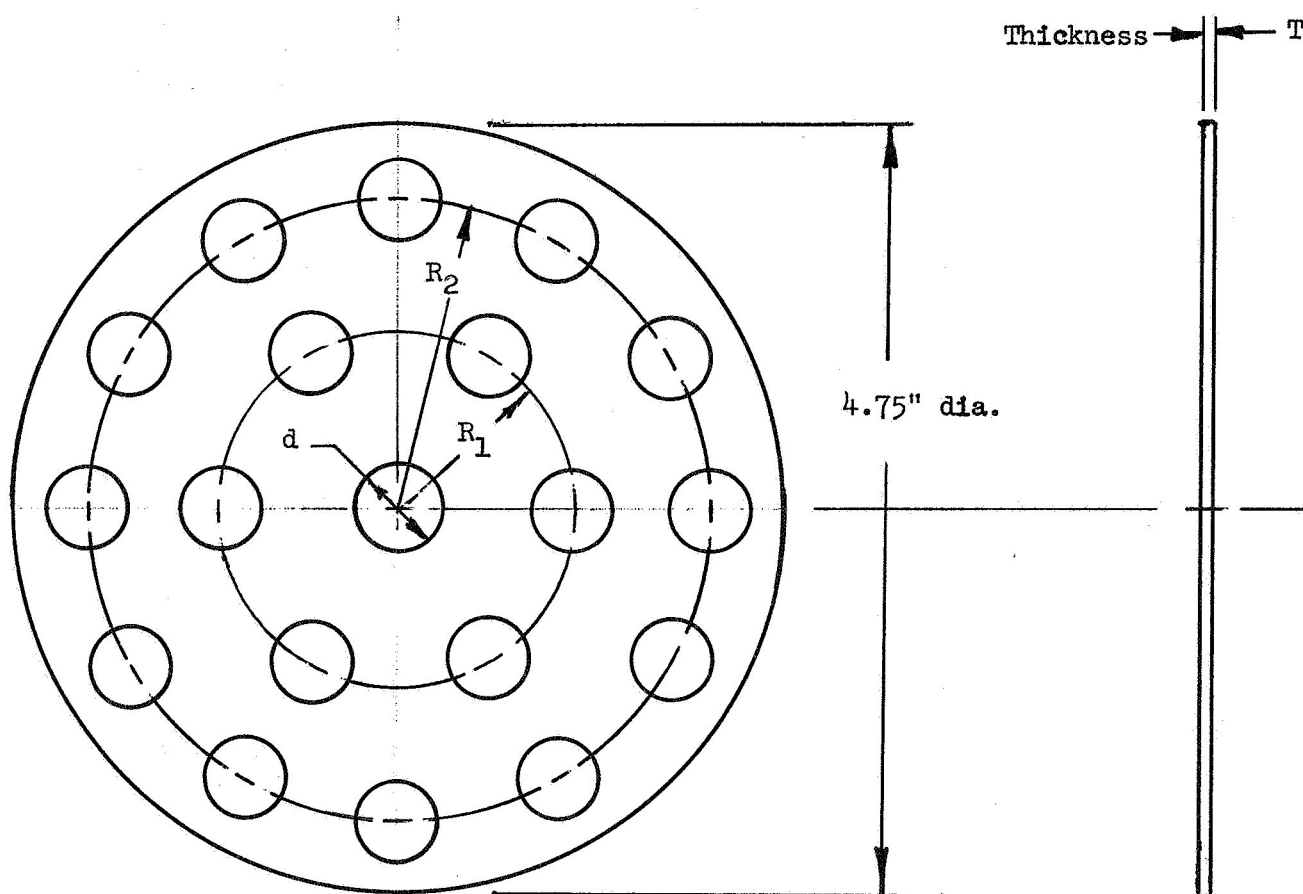


Figure 12: Typical hole layout pattern for plates with constant hole size. (See Table I)

N = Number of holes per hole circle.

Table I: Foraminous Barrier Specifications

[illegible]

Plate No.	Material	R ₁ in.	N ₁	R ₂ in.	N ₂	R ₃ in.	N ₃	d in.	T in.
26	Al	1.56	6					.781	.087
27	Al	1.74	6					.969	.087
28	Al	1.31	6					.656	.087
29	Al	1.62	6					.812	.087
30	Al	1.55	5					.937	.087
31	Al	1.37	6					.687	.087
32	Al	1.80	6					.906	.087
33	Al							3.406	.087
34	Al							3.594	.087
35	Al							2.156	.087
36	Al							2.344	.087
37	Al							2.593	.087
38	Al							2.781	.087
39	Al							4.562	.120

Material Abbreviations: S.S. = stainless steel

Al = aluminum

Br = brass

B. Square Weave Screen Barrier Specifications

Screen No.	Material	Mesh	Wire dia. in.	Open Width in.
S-1	Br.	1	0.192	.808
S-2	S.S.	5/8/2	0.120/.080	.505/.420
S-3	S.S.	2 $\frac{1}{4}$ /2 $\frac{1}{2}$.080/.080/.105	.364/.320/.395
S-4	S.S.	2 $\frac{1}{4}$	0.092	.352
S-5	S.S.	1	0.162	.838
S-6	S.S.	2	0.080	.420
S-7	S.S.	2	0.092	.408
S-8	S.S.	1	0.120	.880
S-9	S.S.	5	0.041	.159
S-10	S.S.	3 $\frac{1}{2}$	0.080	.206
S-11	S.S.	3	0.054	.279
S-12	S.S.	2 $\frac{1}{2}$	0.080	.320
S-13	S.S.	5/8"	0.080	.505

TABLE II. PHYSICAL PROPERTIES - TEST LIQUIDS AND STORABLE PROPELLANTS

PROPELLANTS	T-°C	DENSITY (ρ) lb _m /ft ³	SURFACE TENSION ($\sigma \times 10^3$) lb _f /ft	KINEMATIC SURFACE TENSION ($\beta \times 10^4$) ft ³ /sec ²	CONTACT ANGLE(θ) DEGREES*
A. FUELS:					
Aerozine-50	20	55.5(b)	2.07(b)	12.0	0-2(b)
MMH	-	54.6(c) 24°C	2.35(c) 20°C	13.8	-
UDMH	20	49.4(a)	1.92(a)	12.5	0-45' (a)
MHF-5	20	63.0(d)	2.64(f)	13.5	-
JP-4	20	48.4(e)	1.55(a)	10.3	-
B. OXIDIZERS:					
Nitrogen tetroxide	20	90.6(a)	1.88(a)	6.68	
Nitric Acid (fuming)	20	97.2(b)	3.01(b)	9.98	0-3(a,b)
Chlorine trifluoride	11.7	115.5(g)	1.70(g)	4.74	-
C. MONOPROPELLANTS:					
Hydrogen Peroxide (90%)	20	87.0(b)	5.41(b)	20.0	1-2(b)
Hydrazine	20	62.4(b)	4.33(b)	22.3	0-2(b)
D. TEST LIQUIDS:					
Methanol	20	49.4(e)	1.55(e)	10.1	0(e)
CCl ₄	20	99.6(e)	1.84(e)	5.95	0(e)
Freon TF	20	98.6(e)	1.27(e)	4.15	0(e)

* Contact angles for storables are for Pyrex, 6061-T6 Polished Aluminum, 301 Polished Stainless Steel and ASTM 8348-59T Grade 6 Polished Titanium Alloy; for test liquids they represent contact with Pyrex.

REFERENCES:

- (a) Reynolds, W. C., Saad, M. A., and Satterlee, H. M., "Capillary Hydrostatics and Hydrodynamics at Low-g", Rpt. #T.R. LG-3, Mechanical Engineering Department, Stanford Univ., Stanford, California, September 1964.
- (b) Harris Research Laboratories, "Studies of Interfacial Surface Energies", Summary Report, NASA Contract NAS 3-5744, Report No. NASA CR-54175, December 1964.
- (c) Lawrence, R. W., Handbook of Properties of UDMH and MMH, Aerojet-General Report No. 1292, May, 1958.
- (d) Handbook of Chemistry and Physics, 44th Edition Chemical Publishing Company, Cleveland, Ohio.
- (e) Masica, W. J., et al, Hydrostatic Stability of the Liquid-Vapor Interface in a Gravitational Field, NASA TN D-2267 (May 1964).
- (f) Bell Aerosystems, Evaluation of Propellant Containment and Venting Devices for Zero Gravity Applications, Final Report, Rpt. No. AFRPL-TR-65-118, AF Contract AF 04(611)-9901 (June, 1965).
- (g) Friedman, P. A., and Winkler, J., Properties of Fluorine and Fluorine-Based Propellants, Martin Company Rpt. No. TM-0444-64-8 (Denver, Colorado: July, 1964).

D. Procedure

The glass specimens were washed in a warm detergent solution, rinsed with tap water, and air dried prior to use. The perforated plates and screen barriers were dipped in an acid solution, rinsed with water, and air dried.

The specimens were filled with test fluid to the desired level, attached to the mounting platform and positioned in the inner capsule, Figure 4. The liquid level for the majority of tests was about 1/16-in. to 1/4-in. above the upper-surfaces of the foraminous barriers. A liquid layer was needed to assure complete wetting of the barriers prior to drop initiation. Results from initial tests showed that without a liquid cover overall test setup misalignment could result in the barriers not being completely wetted.

The mounting platform also supported the movie camera, accelerometer and other associated equipment, and was positioned parallel to the top of the inner capsule (within 1/64-in.). The top surface is perpendicular to the capsule's vertical centerline as determined with a transit. The capsule was then balanced so that its centerline was coincident with a vertical line through the capsule's suspension point. The NEG'ATOR spring motors, used to provide the accelerating force, were then attached to the bottom of the capsule on the centerline, so that the force acted along this line during the test. A plumb bob was used to determine the amount and positioning of the balancing weights attached to the top of the capsule.

The spring motors were selected based upon their constancy of force versus linear deflection as determined on a tensile testor (Tinnius Olsen Universal Test Machine). The three motors (5-lb_f nominal, ea) used for the highest acceleration test condition provided an average force of 16.5-lb_f over the deflection range (49-in.). Force variation was less than ± 0.25 -lb_f. The two motors (3-lb_f nominal, ea) used for the mid-range acceleration condition provided an average force of 6.0-lb_f with variations less than ± 0.25 -lb_f over the deflection range of 24-inches. The single motor (0.375-lb_f nominal) used for the lowest acceleration condition provided an average force of 0.435-lb_f with a deviation of ± 0.015 -lb_f over its 6-in. deflection range. The calibrations were made at a deflection rate of 10-in. per min., about one order of magnitude less than that for the actual drops, however, based upon previous experience the calibration results are applicable. The spring motors were checked between drops using a simple spring scale to determine any gross changes in operating characteristics.

A check on the average acceleration of the inner capsule for the entire drop interval was provided by the low-g time obtained and the

total relative travel of the capsules. Low-g initiation and termination were signalled by flash bulbs positioned in the inner capsule in view of the camera.

The inner-capsule acceleration during initial tests was checked by an accelerometer attached to the mounting platform. The meter provided the relative displacement-time relationship of the 0.813-in. steel ball that was recorded on a CEC Model 5-123 recorder located at the second level of the six level laboratory. The ball interrupted current flow in separate photo diode circuits as it passed between the light source and diode. Since the meter is limited to a height of 24-in., at the highest acceleration test condition (0.055-g) the acceleration history is limited to only about 70% of the total drop interval.

After final capsule assembly and evacuation of the drag shield, the package was hoisted to its 75-ft drop height. The drop capsule package was then allowed a period of about five minutes to stabilize itself, and its contents, prior to each drop. Camera and lights were activated about one second, or so, before capsule release to permit the camera to attain constant speed (200 fps) and to provide a one-g reference condition. The transition to the low-g condition, tending to settle liquid from beneath the foraminous material to the opposite end of the cylinders, occurs within approximately 15-milliseconds after severing the single 5/16-in. machine bolt from which the drop capsule package is suspended. Transition from one- to zero-g is near instantaneous.

The general plan was to determine the critical pore size for the test liquids at three different acceleration levels over the range from 0.001- to 0.05-g. Both perforated plates and screens were to be evaluated with emphasis given to the plates. They appear to be more practical due to weight considerations alone for applications where relatively large pore sizes ($d > .10$ -in.) can be used. As a result, more tests were made using plate barriers. The plan was to test a barrier considered stable in one cylindrical specimen with a barrier considered unstable for the same liquid in the other cylinder. Subsequent tests would then be made with pore sizes in the unstable plate reduced and the holes in the stable plate enlarged. A practical minimum change in hole size was selected as 1/32-in. We, therefore, would converge on the critical size in this manner. It was further decided to begin testing at the highest low-g level since the smaller holes could be more easily machined.

III. EXPERIMENTAL RESULTS

A total of 77 data producing drop tests was made. Of these, 14 evaluated pore stability of various square weave screens. The remainder, 63 drop tests, was made for different perforated plate configurations since the primary technical objective was to experimentally verify pore stability of bare, uncoated, perforated barriers.

A summary of all test results is presented in Table III. The foraminous barriers and test liquids are listed for each test. The average acceleration level calculated from the average NEG'ATOR spring force (page 13) and inner-capsule (test cell) mass is presented. Stability results and Bo numbers are also presented. The latter values are based upon pore radius, for the case of perforated plates, and one-half the open dimension, for the square weave screens. Physical property data listed in Table II were used for the three test liquids with no corrections applied to compensate for temperature and pressure differences. The average acceleration was also used in the Bo number calculation.

The stability criteria used to evaluate test results were:

- 1) the pore was stable if no gas were ingested through the barrier during the drop interval; or
- 2) the pore was stable if the liquid-gas interface configuration showed no time dependence during the drop interval.

The first criterion was applicable to the two higher acceleration test conditions while the second was used for the lowest acceleration test condition. These criteria are discussed in more detail in the next section of the report, Chapter IV.

The stable and unstable test data for bare, uncoated, perforated plate barriers are presented in Figure 13. The pore radii tested are plotted against the ratio of kinematic surface tension, β -to-average acceleration, during test. The straight line shown on the plot is the theoretical boundary separating the stable and unstable regions. It is based upon a theoretical critical Bo number of 0.842 based on pore radius. There is some experimental scatter, particularly at the lowest acceleration test condition of 0.0014-g. However, the test data show relatively good verification of the Bo number criterion for hydrostatic pore stability and also fairly good agreement with the theoretical critical Bo number value.

The stability data for the square weave screens are presented similarly in Figure 14. As mentioned earlier, considerably fewer tests were conducted for screens and results are less conclusive than for the perforated plates. Again, the data do verify the Bo number criterion as with the plates, however, the critical Bo number based on the test results is considerably less than the theoretical value of 0.842. A value of 0.450, based on one-half the screen opening, is indicated. Pore size, as presented in Figure 14, is one-half the opening width of the square weave screen. In a previous pore stability investigation of similar type screens under one-g, Ref. 18, one-half the hole opening was used as the pore radius and results agreed with the 0.842 Bond number value. However, the screen holes and wire sizes were at least an order of magnitude smaller than those used in this program. It is believed that this may account for the difference in results. The crimping method used to fabricate square weave screen produces pores that are not orthogonal to the cylinder axis. Also, the circular pore assumption may no longer be valid for the large square openings unless a so-called 'effective' pore radius is used that is less than one-half the square opening. Based upon these somewhat limited data, Figure 14, the effective radius is only about 0.73 that of the one-half open dimension.

Table III: Summary of Test Results

Run No.	Liquid	Barriers				Bond No. ③		Stable		Acceleration a/g
		Left Cyl. No. T, in.	Right Cyl. No. T, in.	Left Cyl.	Right Cyl.	Left Cyl.	Right Cyl.	Left Cyl.	Right Cyl.	
1	F ②	1 0.020	2 0.020	3.19	0.792	No	No			.051
2	F	1 0.020	2 0.020	3.26	0.805	No	No			.051
2a	C	3 0.020	4 0.018	3.14	0.786	No	No			.051
3a	M	5 0.020	6 0.020	3.16	0.802	No	Yes			.051
4a	F	S-1 0.192	S-4 0.092	4.46	0.857	No	No			.051
5a	C	S-5 0.162	S-6 0.080	3.36	0.846	No	No			.051
6a	M	S-7 0.092	S-8 0.120	0.467	2.190	No	No			.051
7a	F	1 ① 0.020	2 0.020	3.26	0.802	No	Yes			.051
8a	C	4 ① 0.018	3 0.020	0.782	3.130	Yes	No			.051
9a	M	6 ① 0.020	5 0.020	0.802	3.160	No	No			.051
10a	F	S-1 ① 0.092	S-4 0.190	4.46	0.859	No	No			.051
11a	C	S-6 ① 0.080	S-5 0.162	0.815	3.36	No	No			.051
12a	M	S-7 ① 0.092	S-8 0.120	0.466	2.19	No	No			.051
13a	M	7 0.032	8 0.032	0.331	0.222	Yes	Yes			.051
				0.287	0.287	Yes	Yes			.051
				0.222	0.331	Yes	Yes			.051
14a	M	8 0.016	7 0.016	0.222	0.331	Yes	Yes			.051
				0.287	0.287	Yes	Yes			.051
				0.331	0.222	Yes	Yes			.051
15a	M	8 0.087	7 0.087	Same	Same	Yes	Yes			.051
16a	F	8 0.087	7 0.087	0.543	0.807	Yes	Yes			.051
				0.675	0.675	Yes	Yes			.051
				0.807	0.543	Yes	Yes			.051
17a	F	8 0.016	7 0.016	Same	Same	Yes	Yes			.051
18a	F	7 0.032	8 0.032	Same	Same	Yes	Yes			.051
19a	C	7 0.032	8 0.032	0.561	0.378	Yes	Yes			.051
				0.464	0.464					.051
				0.378	0.561					.051
20a	C	7 0.016	8 0.016	Same	Same	Yes	Yes			.051
21a	C	7 0.087	8 0.087	Same	Same	Yes	Yes			.051
22a ④	M	7 0.032	7 0.087	0.331	0.331	Yes	Yes			.051
				0.287	0.287					.051
				0.222	0.222					.051
23a ⑤	M	7 0.032	7 0.087	Same	Same	No	No			.051
24a ④	F	7 0.032	7 0.087	0.807	0.807	No	No			.051
				0.675	0.675					.051
				0.543	0.543					.051
26a	M	7 0.125	7 0.190	0.331	0.331	Yes	Yes			.051
				0.287	0.287					.051
				0.222	0.222					.051

Run No.	Liquid	Barriers				Bond No.		Stable		Acceleration
		Left Cyl. No.	Left Cyl. T, in.	Right Cyl. No.	Right Cyl. T, in.	Left Cyl.	Right Cyl.	Left Cyl.	Right Cyl.	
27a	M	7	0.125	7	0.190	0.331 0.287 0.222	0.331 0.287 0.222	Yes	Yes	.051 .051 .051
28a	F	7	0.125	7	0.190	0.807 0.675 0.543	0.807 0.675 0.543	Yes	Yes	.051 .051 .051
29a	M	12	0.087	14	0.087	0.331 0.460 0.695	0.874 1.085 1.325	Yes	Yes	.051 .051 .051
30a	F	12	0.087	14	0.087	0.805 1.110 1.650	2.115 2.560 3.220	No	No	.051 .051 .051
30b	F	12	0.087	14	0.087	Same	Same	No	No	.051
30c	F	12	0.087	14	0.087	Same	Same	No	No	.051
30d	F	12	0.087	14	0.087	Same	Same	No	No	.051
30e	F	12	0.087	14	0.087	Same	Same	No	No	.051
30f	F	12	0.087	14	0.087	Same	Same	No	No	.051
30g	F	12	0.087	14	0.087	Same	Same	No	No	.051
30h	F	12	0.087	14	0.087	Same	Same	No	No	.051
31a	C	12	0.087	14	0.087	0.560 0.780 0.885	1.490 1.855 2.245	Yes	No	.051 .051 .051
31b	C	12	0.087	14	0.087	Same	Same	Yes	No	.051
31c	C	12	0.087	14	0.087	Same	Same	No	No	.051
31d	C	12	0.087	14	0.087	Same	Same	Yes	No	.051
32a	M	S-3	0.080 0.080 0.105	S-2	0.120 0.080	0.369 0.285 0.432	0.710 0.494	Yes	Yes	.051 .051 .051
33a	F	S-3	Same	S-2	Same	0.895 0.695 1.052	1.750 1.210	No	No	.051 .051 .051
34a	C	S-3	Same	S-2	Same	0.624 0.484 0.744	1.220 0.840	No	No	.051 .051 .051
35	C	14	0.190	14	0.032	1.485 1.855	1.485 1.855	No	No	.051 .051
36	F	12	0.190	12	0.032	0.805 1.108	0.805 1.108	No	No	.051 .051
37	F	12	0.032	12	0.190	0.870 1.192	0.870 1.192	No	No	.055 .055
38	F	12	0.032	12	0.190	0.870	0.870	No	No	.055
39	F	8	0.087	12	0.190	0.584 0.675	0.870	Yes	No	.055 .055
40	M	16	0.087	18	0.087	1.640 1.990 2.310	2.640	No	No	.055 .055 .055
41	M	11	0.087	13	0.087	0.890	0.745	Yes	Yes	.055
42	F	9	0.087	10	0.087	0.577	2.520	Yes	No	.055
43	C	21	0.087	22	0.087	0.845	1.805	No	No	.055

Run No.	Liquid	Barriers				Bond No.		Stable		Acceleration
		Left Cyl. No.	T, in.	Right Cyl. No.	T, in.	Left Cyl.	Right Cyl.	Left Cyl.	Right Cyl.	
44	M	15	0.087	17	0.087	0.858	1.178	No	No	.055
45	F	19	0.087	20	0.087	0.726	1.040	Yes	No	.055
46	C	10	0.087	23	0.087	0.985	1.624	No	No	.055
47	M	21	0.087	22	0.087	0.962	1.074	No	No	.055
48	F	24	0.087	21	0.087	0.872	1.30	No	No	.055
49	C	25	0.087	15	0.087	1.122	1.450	No	No	.055
50	M	26	0.087	27	0.087	0.666	1.034	Yes	Yes	.020
51	F	25	0.087	28	0.087	0.578	1.132	Yes	No	.020
52	C	15	0.087	11	0.087	0.570	1.030	Yes	Yes	.020
53	M	29	0.087	30	0.087	0.716	0.970	Yes	Yes	.020
54	F	13	0.087	17	0.087	0.645	1.041	Yes	Yes	.020
55	C	23	0.087	31	0.087	0.642	0.963	Yes	Yes	.020
56	M	11	0.087	32	0.087	0.815	0.939	Yes	Yes	.020
57	F	15	0.087	22	0.087	0.839	0.941	Yes	No	.020
58	C	22	0.087	28	0.087	0.708	0.880	Yes	Yes	.020
65	M	33	0.087	34	0.087	0.899	1.008	Yes	Yes	.0014
66	F	35	0.087	36	0.087	0.864	0.996	Yes	Yes	.0014
67	C	37	0.087	38	0.087	0.880	1.015	Yes	Yes	.0014
77	F	S-12	0.080	S-11	0.054	0.680	0.505	No	No	0.0483
77	F	S-9	0.041	S-10	0.080	0.164	0.254	Yes	Yes	0.0483
78	C	S-12	0.080	S-7	0.092	0.473	0.752	No	No	0.0483
78	C	S-6	0.080	S-4	0.092	0.792	0.565	No	No	0.0483
79	M	S-5	0.162	S-1	0.192	1.870	1.750	No	No	0.0483
79	M	S-13	0.080	S-6	0.080	0.677	0.466	No	No	0.0483
80	F	S-5	0.162	S-1	0.192	1.655	1.540	No	No	0.0175
80	F	S-13	0.080	S-6	0.080	0.596	0.415	No	Yes	0.0175
81	C	S-1	0.192	S-5	0.162	1.540	1.655	No	No	0.0175
81	C	S-6	0.080	S-13	0.080	0.289	0.416	Yes	Yes	0.0175
83	M	33	0.087	39	0.120	0.810	1.460	Yes	No	.00127

- ① The barriers used for these tests were coated with a thin film of Teflon.
- ② Liquid designation: F = Freon T.F.; C = Carbon Tetrachloride; M = Methanol
- ③ Bond Numbers listed are based on pore radius.
- ④ Liquid level was initially 1.0" above the plate.
- ⑤ Liquid level was initially 1.0" below the plate.

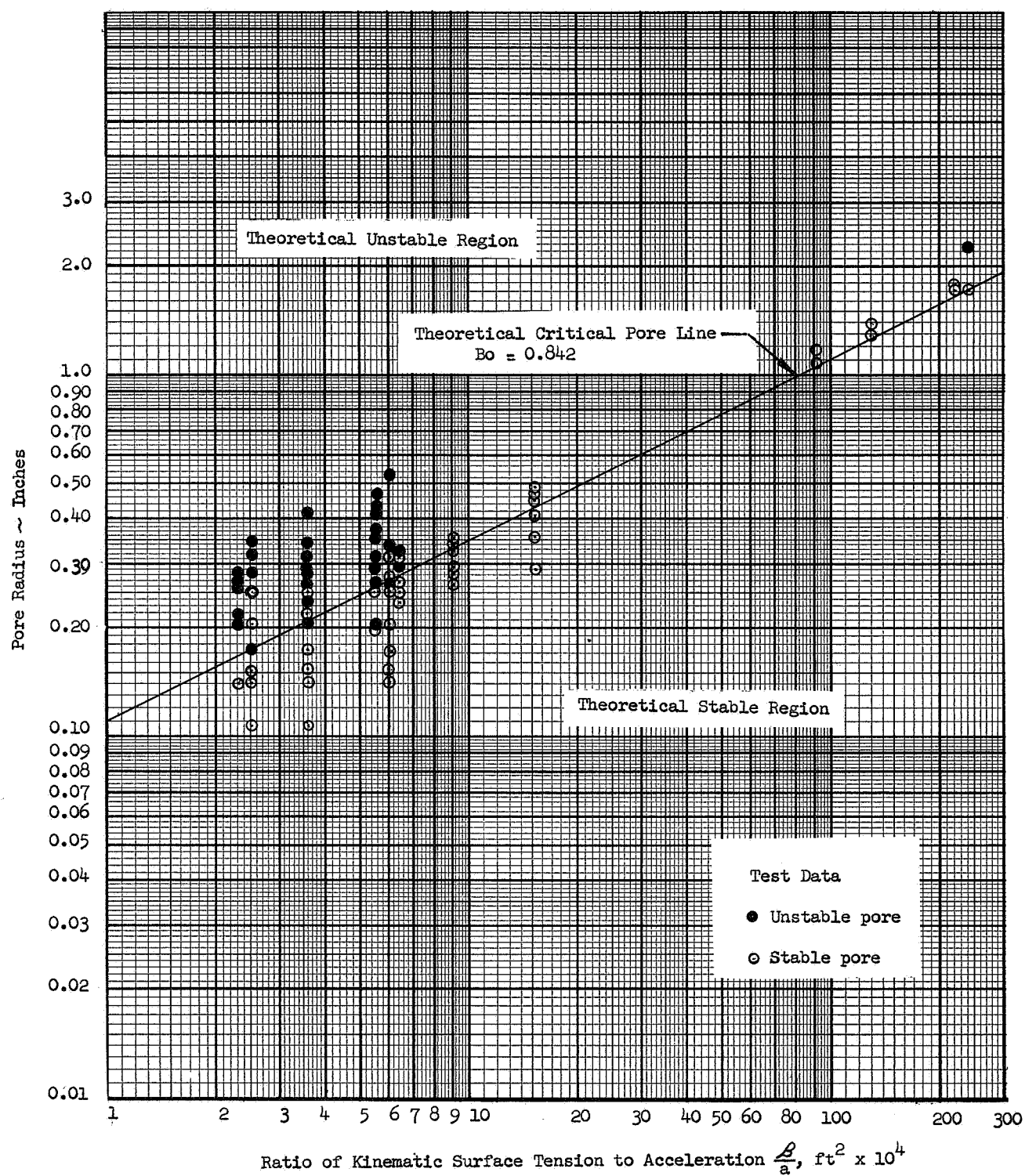
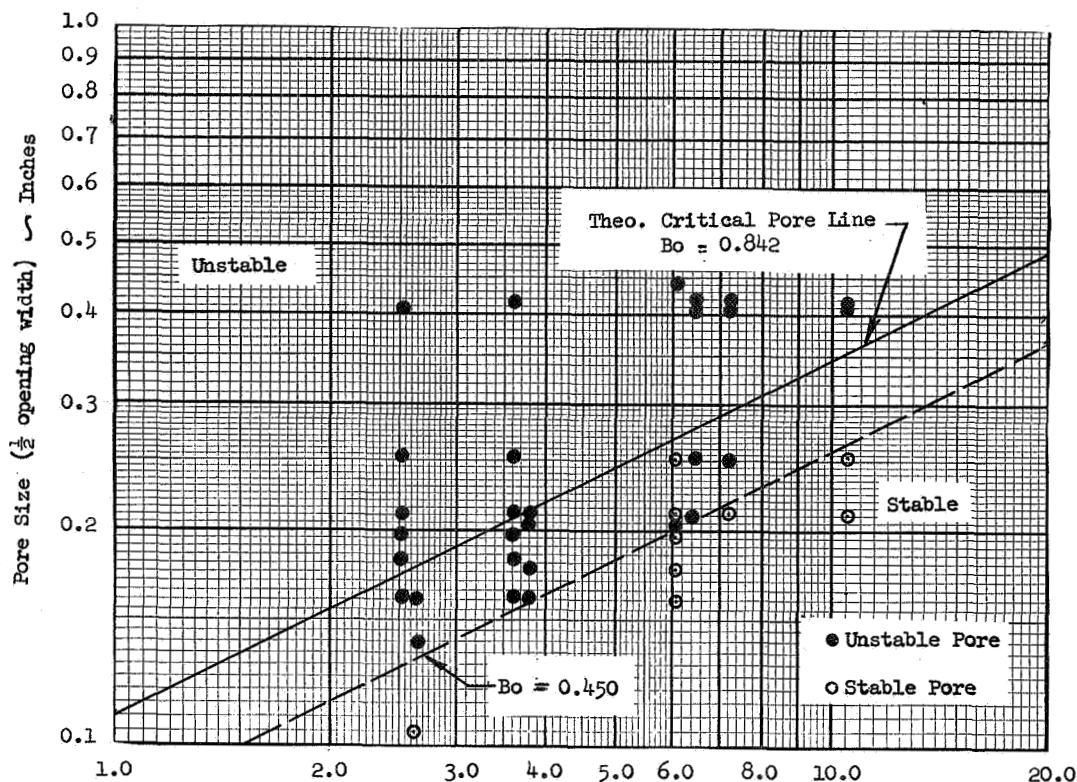


Figure 13: Stability Characteristics for Perforated Plate Barriers



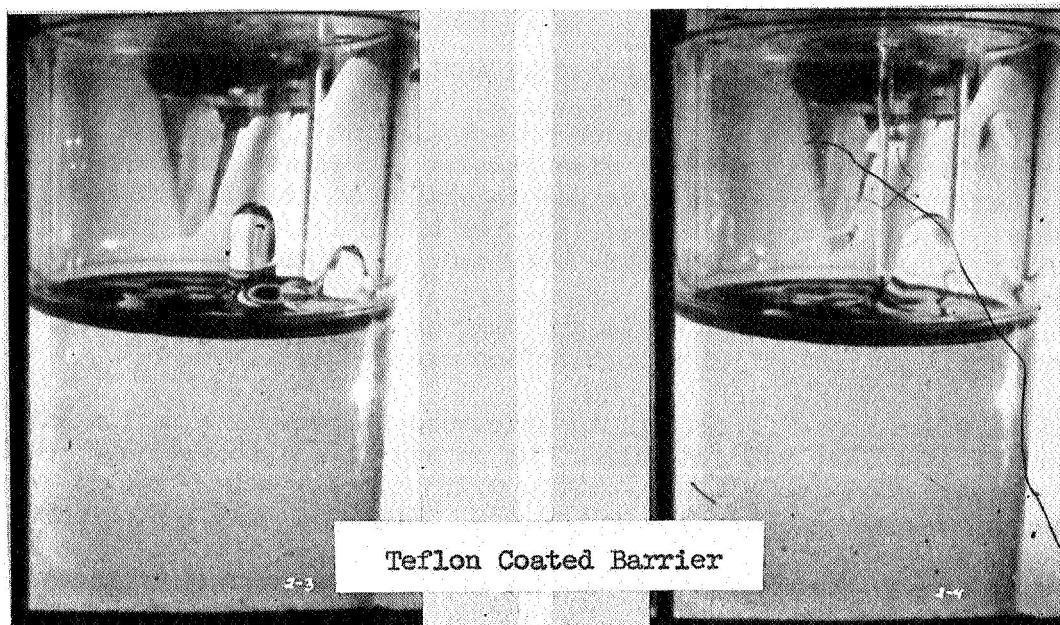
Ratio of Kinematic Surface Tension to Acceleration $\frac{B}{a}$, $\text{ft}^2 \times 10^4$

Figure 14: Stability Characteristics of Square Weave Screen Barriers

In addition to the primary technical objectives mentioned earlier, some consideration was also given to the effect of low surface energy coatings, plate thickness-to-hole size ratio and liquid level beneath the barrier (hydrostatic head) on pore stability.

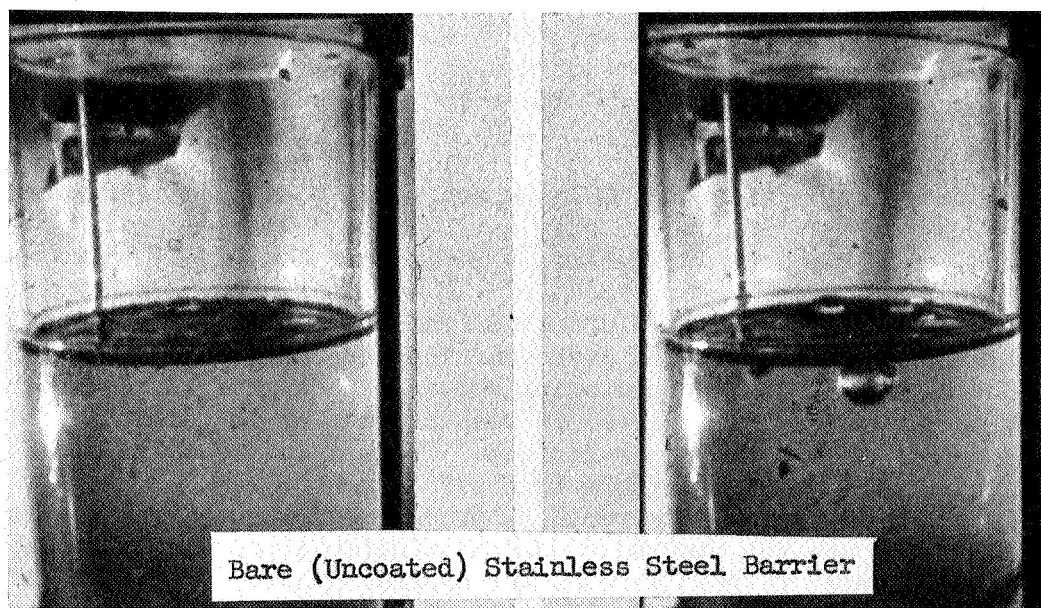
The effect of Teflon coating on barrier performance was briefly investigated for plate and screen barriers during tests 7a through 12a. A thin coat of Teflon, approximately 0.001", was applied to the barriers. Two forms of application were employed. A Teflon resin, E. I. DuPont No. 850-204, requiring a bake period of four hours was applied to the barriers used in runs 7a and 9a. A fluorocarbon spray coating, Miller-Stephenson Chemical Co. No. M.S. 122, was used on the remaining barriers, Run 8a and Runs 10a through 12a.

It appeared that Teflon coating promoted stability considering the results from Runs 2a and 8a, Figure 15. The same plate was unstable when uncoated, Run 2a, but stable when coated with Teflon, Run 8a, under the similar test conditions. The liquid level in Run 8a was, however, above the barrier while in Run 2a it is questionable whether the barrier was wetted. (As discussed in the section covering the test procedure, II.D, the first series of tests, Runs 1 thru 6a, was made with the liquid level just slightly above the upper-surface



$\Delta t = 1.31\text{-sec}$

$\Delta t = 1.91$



$\Delta t = 1.45$

$\Delta t = 2.04$

Figure 15 . Pore stability (Run No. 8a) is pictured in upper photos; instability (Run No. 2a) in lower pictures. Test liquid is CCl_4 and acceleration level is 0.051-g.

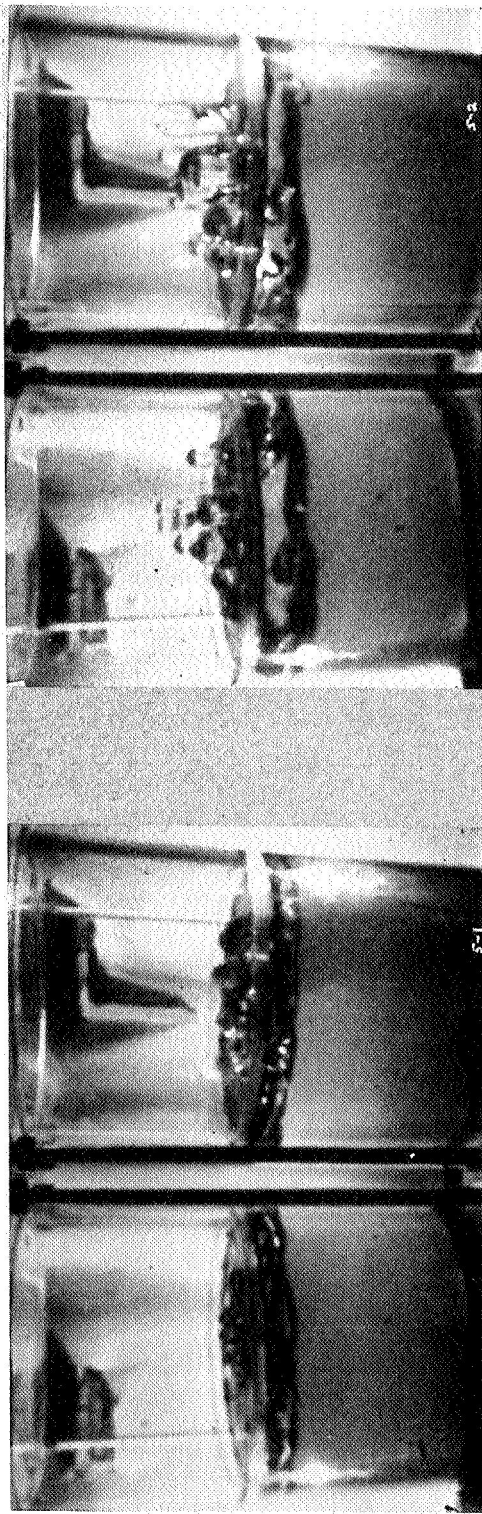
of the barrier, as determined prior to installing the test specimens in the inner-capsule. Filmed results showed, however, that prior to drop initiation the level appeared to actually be slightly below the upper-surfaces due to overall misalignment. Results for most of these early tests showed massive gas ingestion at drop initiation, as shown in Figure 16). The results from Runs 3a and 9a indicated stability with the uncoated plate but not with the coated one, which is contradictory. All of the screen samples tested, with and without coatings, were unstable. Due to the few tests made with low surface energy coatings, no definite conclusions can be made.

The effect of different plate thickness-to-pore size ratios on interface stability was evaluated. As an example, plates #7 and #8 had the same three pore sizes, 0.281, 0.313 and 0.344-in., but different plate thicknesses of 0.016, 0.032, 0.087, 0.125 and 0.190-in. There was no observable effect on interface stability, however, due to these different plate thickness-to-pore size ratios. The amount of liquid above these barriers during stable conditions did appear greater with the thicker plates, however. This result tends to suggest that the liquid-gas interface may have formed at the bottom-surface of the plates rather than at the upper-surface. Also, under unstable conditions, the thicker plates generally required more time to breakdown. As an example, for Run 35 the thicker plate (0.190-in.) appeared to breakdown after about 1.15-sec whereas the thinner plate (0.032-in.) broke down at approximately 0.90-seconds. The test acceleration was 0.051-g.

Plates were studied at a 6-in. hydrostatic head condition except Runs 37, 38 and 39. For these runs only, the head was 4-inches. As expected, based upon the discussion presented in Chapter I, there was no noticeable effect on test results. In addition, Runs 22a and 23a were conducted to observe the effect of the initial liquid level being one-in. above, and below, the plate barrier, respectively. The results from Run 22a, presented in pictorial sequence in Figure 17, show pore interface stability was achieved in both plates for the condition of liquid one-in. above the upper-surface. This is as one would expect since the plates had been stable in previous tests. In Run 23a for the condition one-in. below, Figure 18, liquid passed through the plates initially, but was followed by a condition which appeared to be stable. More liquid seemed to pass through the thinner plate (0.032-in.) during the unstable period. The test condition is, of course, no longer hydrostatic but rather hydrodynamic. The Bo number criterion no longer applies. The criterion now is the We number, a ratio of inertia-to-surface tension forces.

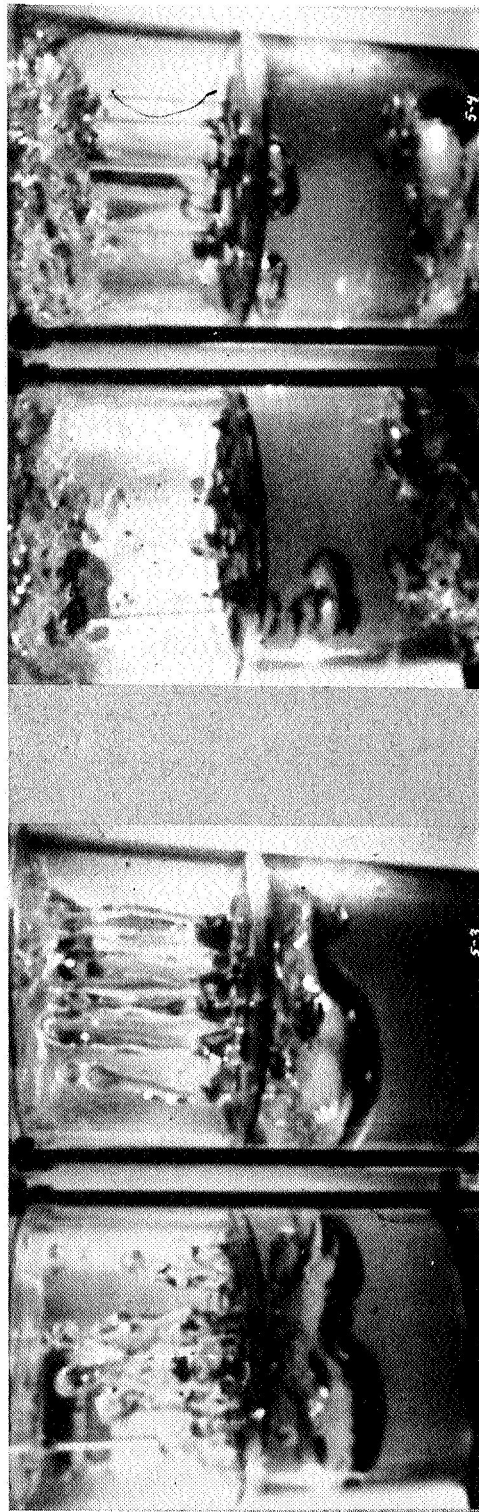
IV. DISCUSSION OF RESULTS

The test procedure, as described in II.D, was for low-g to be initiated with capsule release, i.e., a near-instantaneous transition from one-g (positive) to the low-g (negative) condition. The liquid beneath the foraminous barriers is subjected to a sudden impulse



$\Delta t = 0.595\text{-sec}$

$\Delta t = 0.820$



$\Delta t = 1.19$

$\Delta t = 1.98$

Figure 16 . Filmed sequence of Run No. 2 shows pore instability at 0.051-g for Freon TF, left cylinder w/plate #1 and right cylinder w/plate #2. Rather massive gas ingestion resulted due to liquid not covering upper-surface of perforated plates prior to drop. Liquid columns show good alignment of drop capsule and NEGATOR springs.

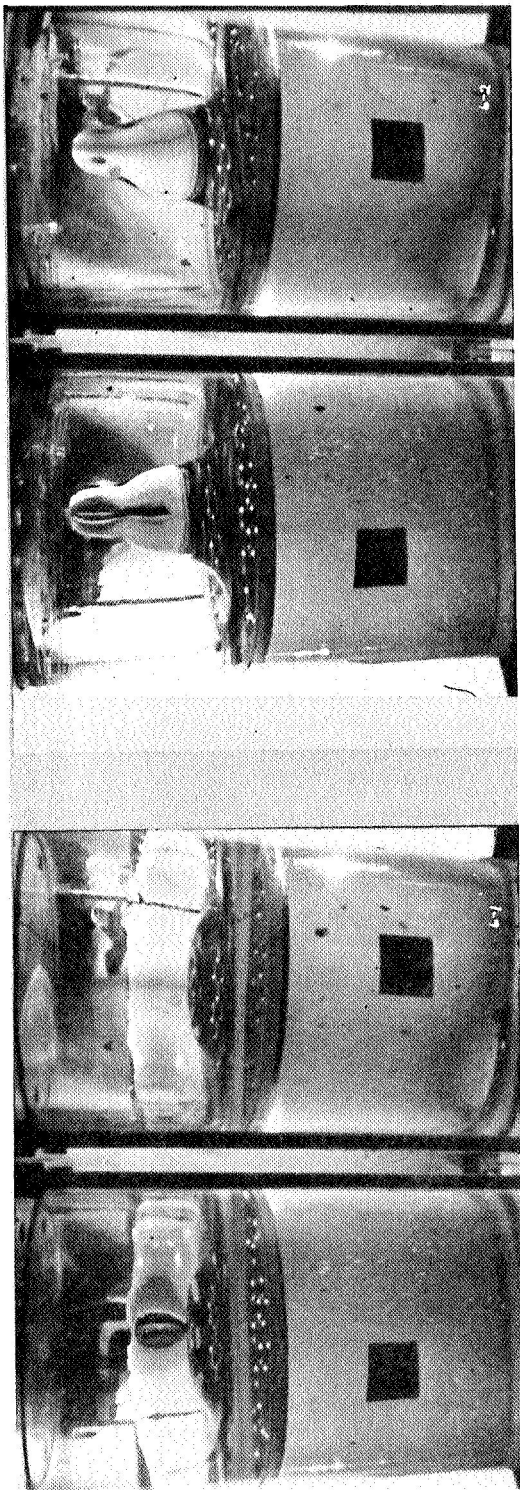
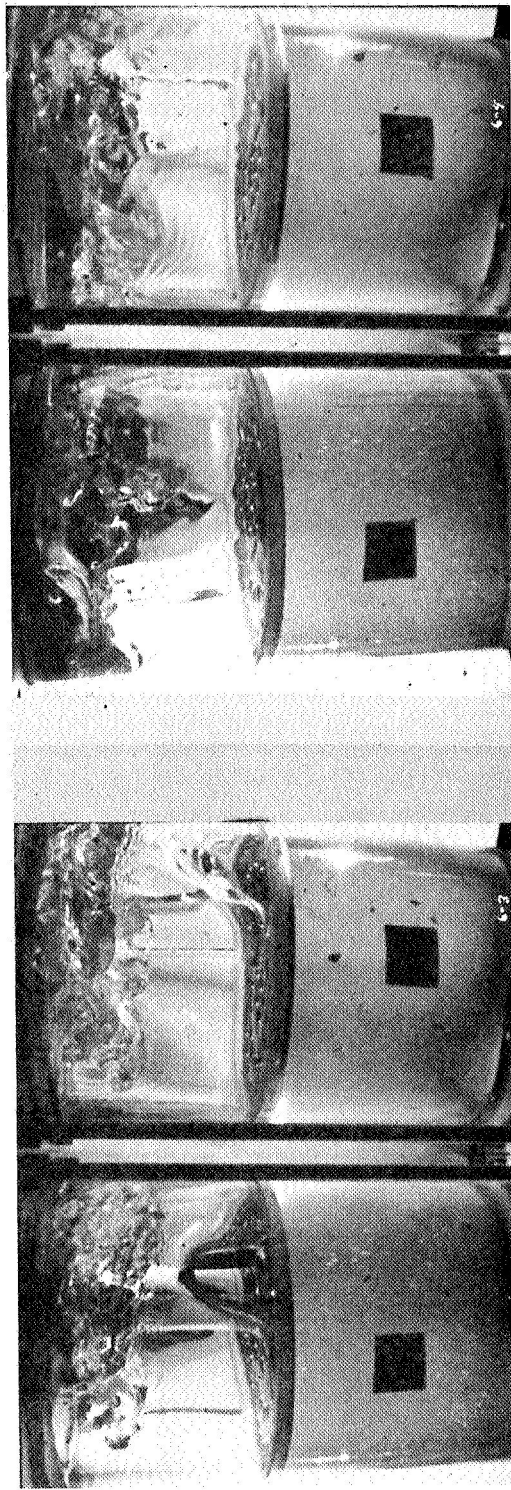
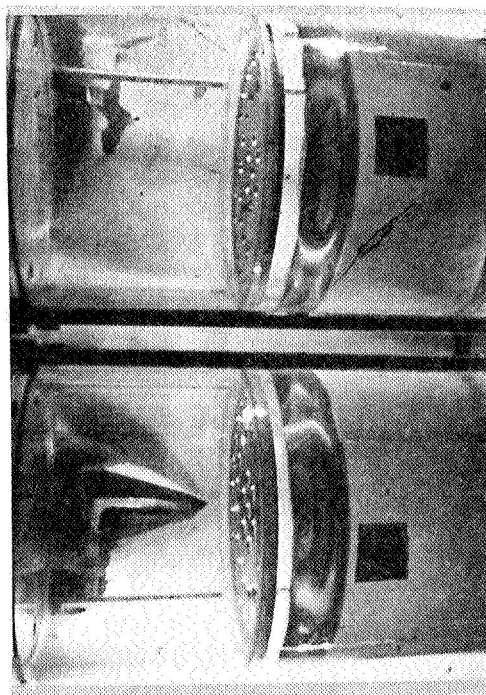
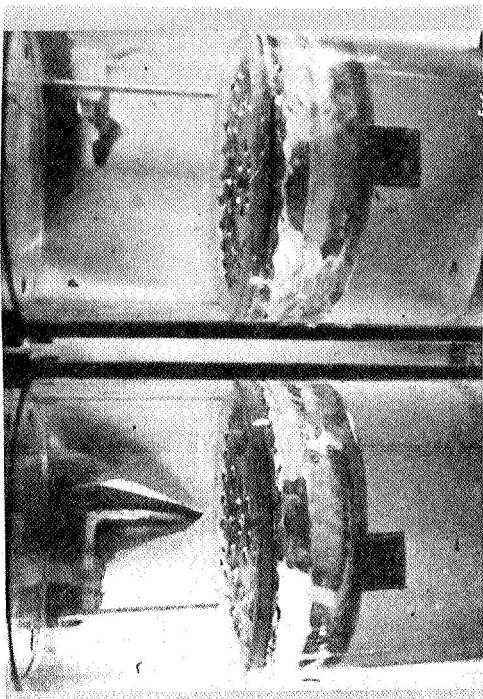

 $\Delta t = 0.440\text{-sec}$
 $\Delta t = 0.820$

 $\Delta t = 1.22$
 $\Delta t = 1.81$

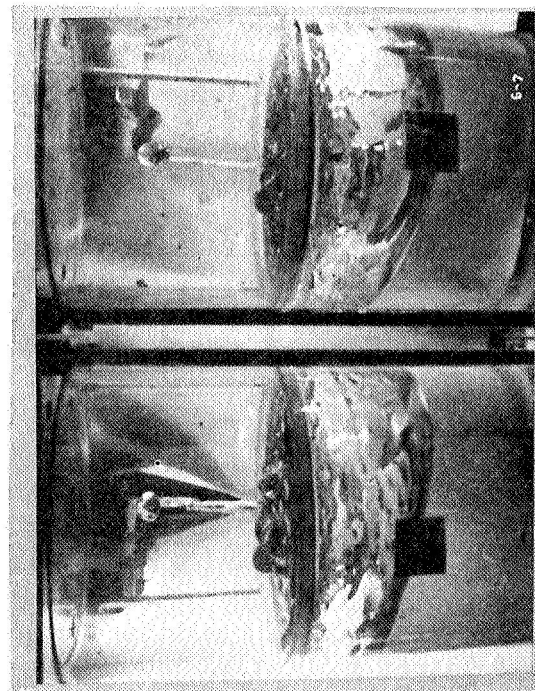
Figure 17. Sequence showing pore stability from Run No. 22a. Test liquid is methanol; g-level is 0.051-g. Cylinders are filled to a



$\Delta t = 0.330\text{-sec}$



$\Delta t = 0.695$



$\Delta t = 1.067$



$\Delta t = 1.84$

Figure 18. Filmed sequence shows results of Run No. 23a. Low-g level is 0.051-g, test liquid is methanol, and plate #7 is in each cylinder. Liquid level before drop is one-in. below perforated plates. The central liquid dome shown at 0.695-sec penetrates both perforated barriers ($\Delta t = 1.067$), however, at 1.84-sec it appears that plates have been wetted and initial ullage is trapped beneath barriers.

tending to settle liquid through the flat barriers to the opposite tank-end.* The drop tests simulated the desired engine shutdown condition except that the change in acceleration (from one- to zero-g) is several orders of magnitude shorter than the probable in-space occurrence. For example, the Titan Transtage main engine thrust tailoff occurs over a one-sec interval with typical thrust decay from 16,000- to 2,000-lb_f occurring during the initial 0.4-second. The drop tower transition period is near-instantaneous. Zero-g is effected by shearing a bolt that supports the capsule package prior to the drop. This near-instantaneous acceleration change tends to present a more severe condition on pore stability due to possible fluid motion caused by liquid compression and structural relaxation phenomena. Liquid compression is analogous to a compressed spring. If the compression is released quickly, compression energy is transformed entirely to kinetic energy and the spring jumps. If compression is released more slowly, the spring tends to accommodate to the changing force and merely expands. The second phenomenon, structural relaxation, results from load bearing material deflecting to attain new equilibrium positions following a change in acceleration. As mentioned, both phenomena tend to cause unwanted initial fluid motion in the hydrostatic stability tests. The filmed test results, however, showed little, or no, fluid motion during drop initiation. This negligible effect resulted because the test liquids possess relatively low liquid compression response times and corresponding maximum velocities, on the order of 0.5-milliseconds and 0.09-in/sec, respectively, based on the analytical method outlined in Ref. 22. Also, the drop capsule hardware was built to minimize relaxation effects, Ref. 23. The foraminous barriers, Table I, and the thick-wall ($\frac{1}{4}$ -in.) cylindrical specimens were also relatively stiff and rigid.

The magnitude of the drop test acceleration change, one-g, corresponds to a probable space operation, again based upon the Transtage.

As discussed in Parts C and D, Chapter II, the test liquids were chosen and cleaning methods used to provide data applicable to storable propellants. Care was also exercised, Chapter II.D, to provide the desired axisymmetric settling acceleration conditions. The liquid settling flow regimes observed during the program tend to substantiate the axisymmetric case. For the majority of tests, liquid motion was symmetrical tending to suggest that the accelerating force was axisymmetric (to within one degree) based upon the liquid resettling results obtained during the CLEO Program, Contract NAS8-11328. During the latter program, off-axis accelerations of one degree caused definite unsymmetric liquid motion during resettling.

The terms, positive and negative, are used to denote direction of the acceleration vector. The negative case tends to relocate liquid from beneath the barrier to the opposite end of the cylindrical specimen whereas the positive acceleration acts in the opposite direction tending to oppose liquid relocation.

The method suggested in Ref. 24 for single-sample experiments was used to provide some measure of reliability for the test results. The second-power equation (equation 7, Ref. 24) was used to estimate the accuracy of the Bo number determination:

$$w_{Bo} = \left[\left(\frac{\partial Bo}{\partial \sigma} w_{\sigma} \right)^2 + \left(\frac{\partial Bo}{\partial m} w_m \right)^2 + \left(\frac{\partial Bo}{\partial R} w_R \right)^2 + \left(\frac{\partial Bo}{\partial f} w_f \right)^2 + \left(\frac{\partial Bo}{\partial \rho} w_{\rho} \right)^2 \right]^{\frac{1}{2}} \quad (3)$$

where w is the uncertainty interval, plus or minus, associated with the Bo number and the variables in the Bo number relationship:

$$Bo = \frac{\rho f R^2}{m \sigma} \quad (4)$$

where ρ is liquid density; f is average NEG'ATOR spring force; R is pore radius; m is drop capsule mass; and σ is liquid-vapor surface tension. Equation (3) is valid only when the uncertainties associated with each variable are based upon the same odds. These uncertainties are presented for the variables in the Bo number relationship at low-g test conditions in Table IV. They are based upon probable odds of 20:1. In other words, the best value for each variable is the average value and the odds are 20:1 that the true value lies within the uncertainties, as listed.

Table IV. Pertinent Variables and Their Uncertainty Intervals

A. Representative of 0.051-g Condition

<u>Variable</u>	<u>Symbol</u>	<u>Ave. Value</u>	<u>Uncertainty Interval (w)</u>
Accelerating force	f	16.5 lb _f	± 0.25 lb _f
Test cell mass	m	324.0 lb _m	± 1.0 lb _m
Liquid density	ρ	49.4 lb _m /cu ft	± 0.5 lb _m /cu ft
Liquid-gas surface tension	σ	22.6 dyne/cm	± 1.0 dyne/cm
Pore radius	R	0.141 in.	± 0.003 in.

B. Representative of 0.020-g Condition*

<u>Variable</u>	<u>Symbol</u>	<u>Ave. Value</u>	<u>Uncertainty Interval (w)</u>
Accelerating force	f	6.0	± 0.25
Test cell mass	m	300.0	± 1.0
Pore radius	R	0.391	± 0.003

C. Representative of 0.00145-g Condition*

<u>Variable</u>	<u>Symbol</u>	<u>Ave. Value</u>	<u>Uncertainty Interval (w)</u>
Accelerating force	f	0.435	± 0.015
Test cell mass	m	300.0	± 1.0
Pore radius	R	1.703	± 0.003

*Liquid density and surface tension values are the same at all g-levels. The test liquid is methanol.

Partial differentiation of the Bo relationship with respect to each of the variables and non-dimensionalizing the second order uncertainty equation by dividing by the Bo number yields:

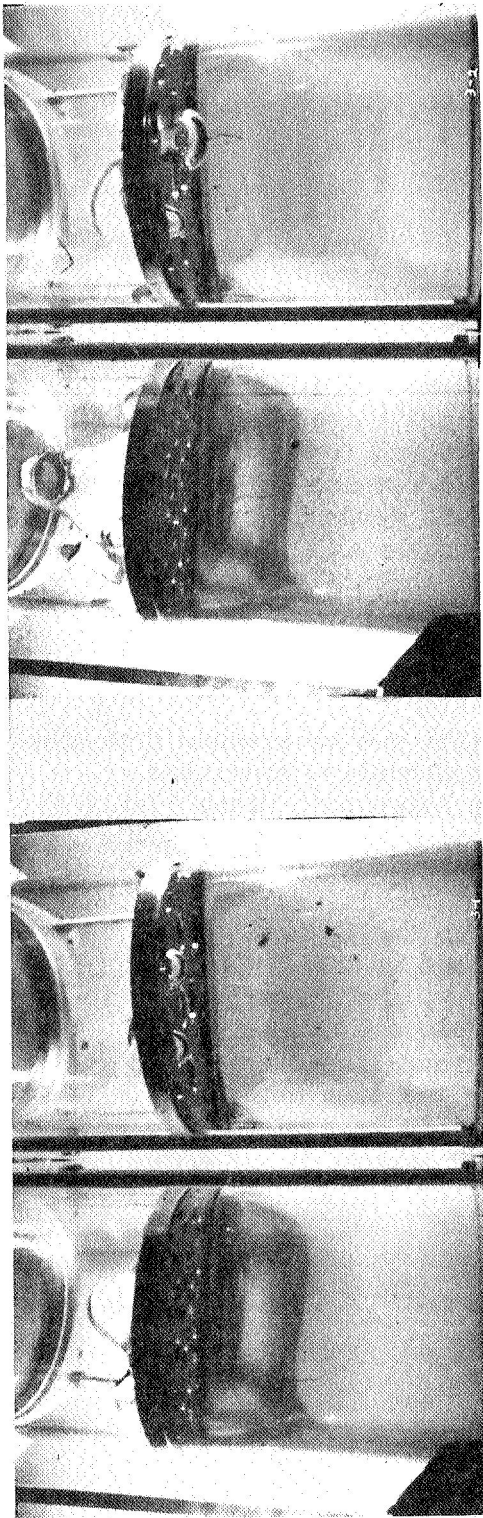
$$\frac{w_{Bo}}{Bo} = \left[\left(\frac{w_{\sigma}}{\sigma} \right)^2 + \left(\frac{w_m}{m} \right)^2 + \left(\frac{2w_R}{R} \right)^2 + \left(\frac{w_f}{f} \right)^2 + \left(\frac{w_{\rho}}{\rho} \right)^2 \right]^{\frac{1}{2}} \quad (5)$$

Substitution of the average values and uncertainty intervals (Table IV) for each of the variables provided the following Bo number uncertainty limits at the three basic low-g test conditions. The uncertainties are $\pm 6.3\%$ at $.051\text{-g}$, $\pm 6.2\%$ at 0.020-g , and $\pm 5.6\%$ at $.0014\text{-g}$. The numbers were calculated using methanol properties and the smallest pore sizes used with methanol for tests. The ranges are representative of the other test liquids, Freon TF and carbon tetrachloride, and pore sizes, as well. It is interesting that at the lowest g-level probable inaccuracies in surface tension and acceleration force were the more significant, contributing about equally to the Bo number uncertainty. At 0.02-g , this again was the case. Whereas at 0.051-g , pore size and surface tension variations were the critical variables in determining Bo number reliability.

The stability, or instability, of a given foraminous barrier was determined from the 16-mm color film documenting the entire drop test interval. Stability criteria were by definition either that no gas was ingested through the pores of the foraminous material into the liquid beneath the material or that the interface configuration was independent of time during the drop interval.

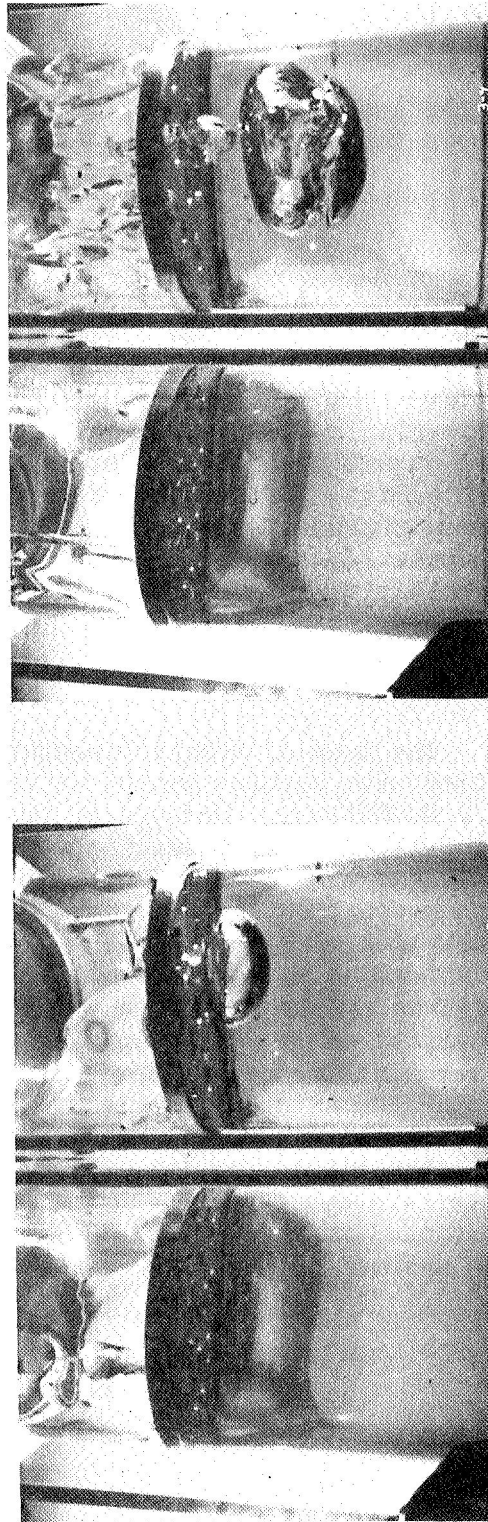
Typical of the gas ingestion criterion is the photo sequence presented in Figure 19. Several, or more, bubble sites are evident in the cylinder at the right at $\Delta t = 0.976\text{-sec}$, however, as shown in the subsequent photos only one bubble grew and detached. Other runs showing gas ingestion were similar except that two or three bubbles from a number of initial bubbles grew to critical size (bubble radius equal to the effective pore radius) and detached. The liquid-gas interface changes during the drop because of the interfacial elastic membrane tending towards its minimum gas-liquid area (minimum surface energy) and because of the buoyant force acting on the curved interface at each pore of the barrier. Due possibly to slight variations in pore size, and/or uneven liquid cover over the barrier*, one, or maybe only

*As mentioned, a liquid cover was used to assure that the plates and screens were completely wetted for each test. The motion of this liquid during low-g was similar to that studied by Dr. T. E. Bowman during the CLEO Program, Contract NAS8-11328. Liquid tends to resettle to the top of the test specimens by flowing along the wall and moving in a central liquid column or dome. The latter formation at the higher low-g conditions resulted in liquid covering the central portion of the barriers. Breakdown or pore instability, in general, occurred only in the pores in the largest pore circle (nearest the wall). Plates such as #7 and #8 (Table I) that had different pore sizes, therefore, did not provide the results desired. Growth and existence of the liquid dome prevented gas-liquid interfaces at the pores in the central plate region. Instead of providing test data for three different Bo numbers for each plate, stability data for the pores on the outer-circle only were obtained.



$\Delta t = 0.976\text{-sec}$

$\Delta t = 1.23$



$\Delta t = 1.45$

$\Delta t = 1.90$

Figure 19. Sequence shows bubble formation during pore instability during Run No. 31d at 0.051-g. Test liquid is CCl_4 . Although several bubble sites are formed in the right test specimen, only one grows and detaches from the perforated plate.

several, gas bubbles tend to reach critical bubble size at about the same time. Bubble pressure is inversely proportional to its radius of curvature (Ref. 25):

$$(\Delta P)_B = \sigma \left(\frac{1}{R_1} + \frac{1}{R_2} \right) \cos \theta \quad (6)$$

or for a spherical interface ($R = R_1 = R_2$) the pressure difference across the bubble surface, $(\Delta P)_B$, is simply;

$$(\Delta P)_B = \frac{2\sigma}{R} \quad (7)$$

neglecting contact angle effects. At drop initiation when there is little or no curvature of the pore interface, the radius of curvature approaches infinity and the bubble pressure is near-zero. As the low-g condition continues, the interface becomes curved with the radius of curvature decreasing so that differential bubble pressure increases to a maximum that occurs when the radius of curvature is equal to the effective pore radius. Once this pressure condition is attained, the curvature moves towards a spherical shape and the bubble tends to detach. Once a bubble leaves, as in Figure 19, bubble breakthrough tends to continue at that site in preference to developing new instability areas. As discussed in Ref. 26, a supplementary force acts on new bubbles being formed due to tearoff and motion of the bubbles that have already left the barrier surface.

The type of bubble breakthrough discussed was observable from the filmed test results except at the lowest acceleration condition ($a = 0.0014g$). Because of the relatively large pore sizes (Table I) and 5-in. I.D. test specimens, the perforated plate barriers could contain a single pore only. Instability was, therefore, a different phenomenon than at the other drop tower test conditions. Rather than observance of gas breakthrough, the interface configuration was observed to determine whether or not it was independent of time. If it was, the pore was considered to be stable. Conversely, the criterion for instability was that the interface be time dependent during the drop test interval. Both the interface configuration and liquid motion up the walls of the container were observed to establish the time dependence. Of the two, the liquid motion along the walls could be determined more accurately from the filmed results. When this velocity slowed to zero, the interface configuration was assumed to be stable. If the liquid layer continued to move upward along the walls, the interface configuration was assumed to be unstable.

V. CONCLUSIONS AND RECOMMENDATIONS

A. Conclusions

The results of this program are directly applicable to the design of capillary systems to control fluids during low-g operation. The designer must possess these criteria to select foraminous material that will assure satisfactory and reliable system operation. As an example, let's look at a storable, liquid propellant storage system that might have application for an interplanetary mission, Figure 20. The compartmented capillary design is representative of a mission during which there are several major liquid expulsion demands (two course corrections and an orbit insertion) and propellant center-of-mass, c.m., control is a requirement. Venting is not a consideration since it is assumed that the propellants are storable such as nitrogen tetroxide and monomethylhydrazine.

The perforated bulkheads are intended to provide c.m. control, and are positioned at the location of the liquid free surface prior to each major draining. Initial ullage is above plate 1. The first burn will empty the tank to plate 2; the second burn to plate 3; with the final burn emptying the tank. The plates serve as one-way check valves permitting pressurization gas to enter each compartment to displace propellant during each draining while maintaining propellant beneath the perforated plates. The position of the plates, except for 1, will undoubtedly only be known to some degree of tolerance. As a result, based upon the results of this program, these plates should be positioned to assure a liquid cover.

It may also be desirable to use a screen or perforated plate liner, as in Figure 20, or at least a perforated segment over the outlet to prevent suction dip (Ref. 27) during the last draining. A perforated liner, in addition to preventing suction dip, will also provide liquid draining if ullage were to accrue beneath plate 3 prior to the last expulsion, Ref. 15.

B. Recommendations

No additional hydrostatic stability tests are recommended for perforated plate barriers. It may be desirable to further substantiate

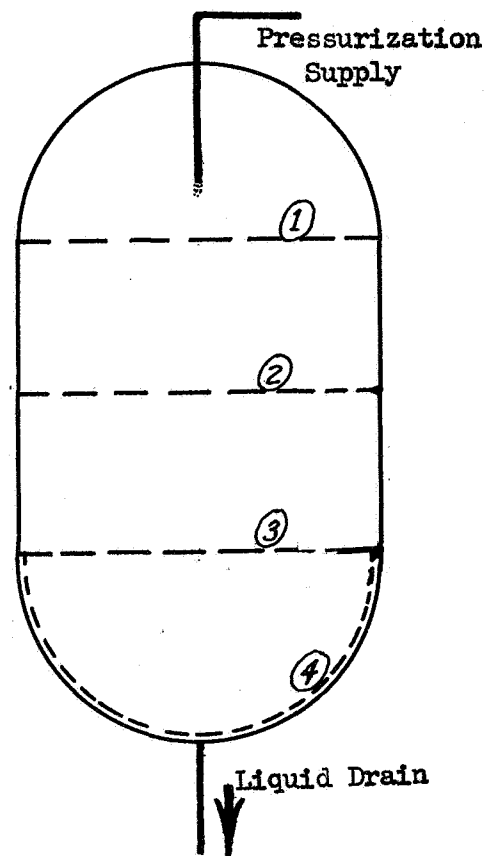


Figure 20: Compartmented Tank With Perforated Partitions

the critical Bo value for square weave screens. However, their application as propellant containment devices does not appear to be as promising, due to weight and fabrication considerations, when compared to perforated plate.

It is recommended that damping capability of perforated plates, when the liquid level is some distance beneath the plate, be investigated further. This condition was investigated in several drop tests during this program. The results of one test, Run 23a, is pictured in Figure 18. The hydrostatic Bo number criterion, as seen, no longer applies but rather the We number (based on pore size) is now the stability criterion. This should be verified experimentally and critical values established. The effect of several different plate contours (other than flat) should be studied. For example, based upon the results presented in Figure 17, baffle-like plates, Figure 21, would appear to be more effective. The ring segment at the tank wall and the solid section in the center of the baffle would tend to prevent liquid flowing along the walls or in a central liquid dome from leaving the trap during liquid resettling. The foraminous section again would serve as a one-way check valve, as described earlier.

Stability has been verified under one-g and high-g in a centrifuge for Dutch-Twill screen (Ref. 15) and for perforated plate under one-g (Ref. 3) with the acceleration parallel to the screen. This is a more severe vector direction since capillary forces alone now must stabilize the free surface interface. Ullage pressure no longer supports the liquid. This stability phenomenon should be verified for perforated plate under low-g. It is understood that MSFC is presently conducting such a drop tower study (Ref. 28).

Another capillary design area needing additional drop tower verification is annulus refill. The ability to off-load propellant in a capillary system is an attractive feature. (It is not desirable to off-load metallic and non-metallic bladders.) For example referring to Figure 20, the tank could be loaded to any level. If this level were beneath plate 3, the tank must be exposed to a low-g condition for a sufficient time interval to allow surface tension to fill the screen liner (screen 4). Time required for capillary forces to fill an annulus, as in Figures 20 and 21, and degree of filling as functions of pore size, annulus gap size, and acceleration level need further verification.

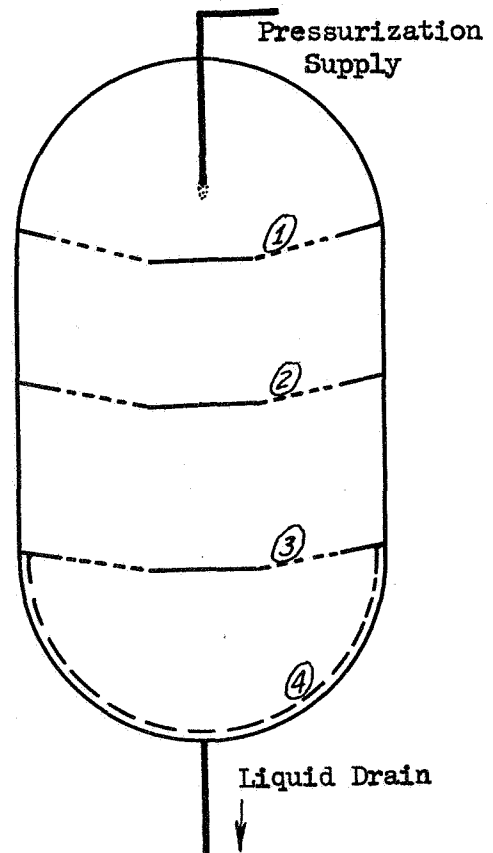


Figure 21: Compartmented Tank With Baffle-Like Partitions.

These additional data will have general application to capillary control systems. Subsequent to the drop tower investigations recommended here, orbital experiments that would provide test periods several orders of magnitude longer than those obtainable in drop towers are needed to qualify capillary systems for flight applications. The longer test duration is required to completely drain a tank and to evaluate liquid slosh and fluid c.m. control. Therefore, NASA support of an orbital experiment for inclusion in the Apollo Applications Program is recommended. The experiment would be designed to provide quantitative data with regard to flow losses (pressure drop), liquid expulsion efficiency for different expulsion schedules, i.e., flowrate and delivery intervals, annulus refill, and at least qualitative visual results with regard to slosh and c.m. control. The program would benefit other capillary system areas presently under investigation such as tank loading and fabrication of the foraminous material. These areas would benefit during the preliminary work leading to the orbital test. Since it will require about six months to define a program and make preliminary designs, and about another year to finalize designs, fabricate the experiment and perform system checkout tests, the program should be initiated during 1968, preferably by mid-year. This early attention is needed to facilitate submittal of the experiment plan, NASA Form 1138, to MSFEB, NASA Headquarters, for consideration in the AAP Program. As seen in Table V, there are several missions, beginning in April '70, that could serve as the orbital test bed.

Saturn I Launches	CY 1970												CY 1971											
	J	F	M	A	M	J	J	A	S	O	N	D	J	F	M	A	M	J	J	A	S	O	N	D
				▲				▲					▲		▲		▲	▲						
Flight Number				207				209					210		212		213	214						
AAP Number				1				3a					3		5		6	7						
				△									△											
Flight Number				208									211											
AAP Number				2									4											
				WS									ATM											
Legend: ▲ - Manned WS - Workshop △ - Unmanned ATM - Apollo Telescope Mount																								

Table V: Apollo Applications Program Launch
Schedule, December 19, 1967

The type of experiment proposed is shown in Figure 22. Both tanks, about one-ft in size, would contain capillary devices. Tank sizes will be chosen to keep the outside dimensions of the package within 20" x 25" x 40" per the AAP guideline. Only one tank, preferably the multiple screen configuration would be loaded on the ground. Astronauts would carry the experiment package from the Multiple Docking Adapter (MDA) into the Orbital Workshop (WS). The in-space test procedure would be to expel a substitute liquid, probably methanol since a storable propellant can't be used due to AAP limitations, in multiple drainings to the receiver tank. After expulsion is complete, liquid would then be expelled back into the original storage tank and the draining sequence continued at different expulsion rates. Astronauts would monitor the expulsion tests. A flow transducer, such as the RAMAPO Mark V, would be used to sense rate of fluid flow. The Mark V model senses flow rate as a product of the dynamic forces acting upon a fixed body immersed in the flow stream. Since the transducer measures a drag force, a function of fluid density, whether a single-phase liquid is drained, or not, should be determinable. A sight glass would also be used to determine single phase flow. The multiple screen tank will limit visual observation and photographic coverage to sight ports only. Contents of the cylindrical tank could be documented, however, to evaluate slosh and fluid control. This fluid motion and control would be monitored by an astronaut using a 16 mm camera. Pressures and temperatures will be measured. Sensitive, three-axes accelerometers will be used, if needed, to provide an acceleration history to correlate the quantitative test results.

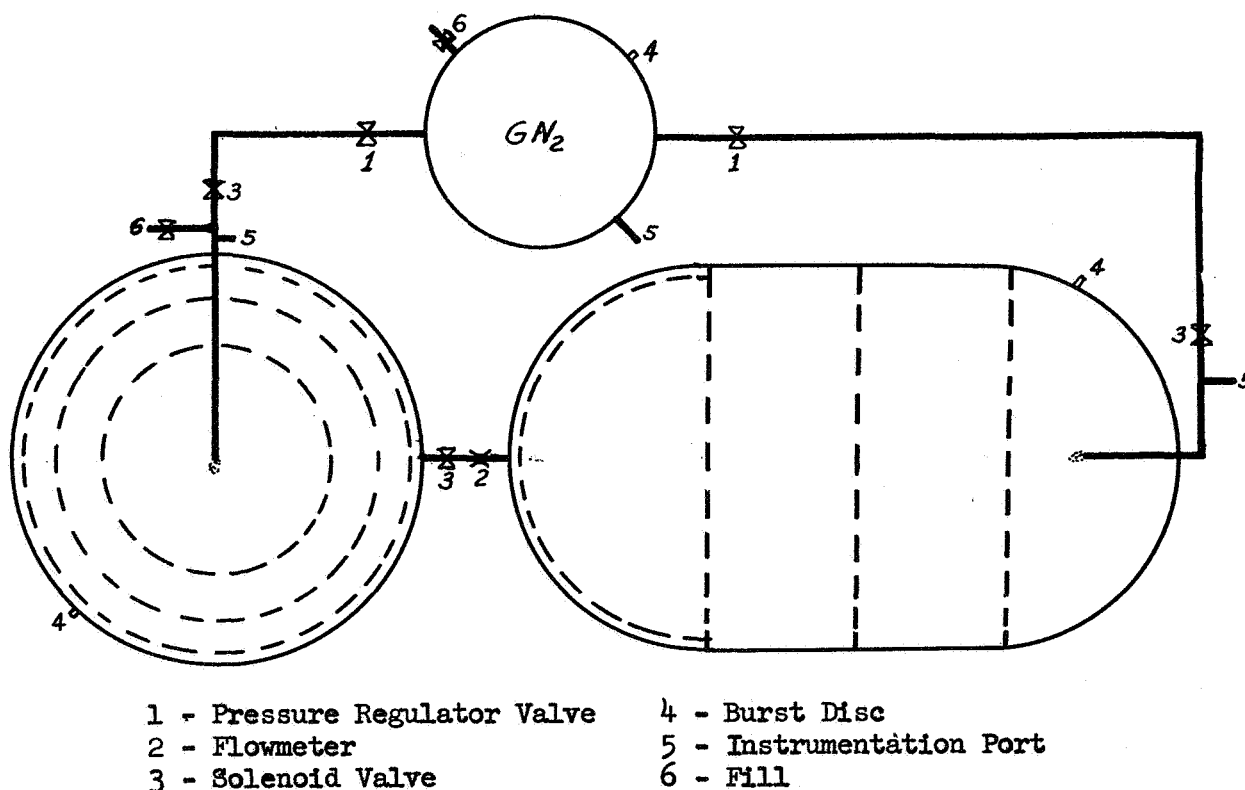


Figure 22: Martin Marietta Proposed Orbital Experiment

VI. REFERENCES

1. R. G. Clodfelter and R. C. Lewis: Fluid Studies in a Zero-Gravity Environment. ASD Technical Note 61-84, June 1961.
2. H. L. Paynter: Analysis of Liquid Containment With Screens in Zero-G. IDC-1324-247-61. Martin-Marietta, Denver Division, Denver, Colorado, 14 June 1961.
3. Phase I Report, Development of Expulsion and Orientation Systems for Advanced Liquid Rocket Propulsion Systems. Contract AF 04(611)-8200. Report No. SSD-TDR-62-172, Bell Aerosystems Company, December 1962.
4. Final Report, Evaluation of Propellant Containment and Venting Devices for Zero-Gravity Application. Contract AF 04(611)-9901. Report No. AFRPL-TR-65-118, Bell Aerosystems Company, June 1965.
5. H. L. Paynter: "Capillary Devices for Providing Positive Expulsion of Liquid Propellant in Zero-g". Paper presented at Symposium on Positive Expulsion Propellant Systems for Space Vehicles, Aerospace Corporation, Los Angeles, California, 26 March 1964.
6. H. L. Paynter, et al: "Zero-g Liquid Propellant Orientation by Passive Control". Paper 862D presented at SAE-ASME Air Transport and Space Meeting, New York, April 1964.
7. J. D. Doub: ACS Zero-g Reservoir Design Report, Phase I. Contract AF 04(611)-150. TM-III-65-17, Martin Marietta, Denver Division, Denver, Colorado, October 1965.
8. M. A. Saad and S. C. DeBrock: "Simulation of Fluid Flow Phenomena in Propellant Tanks at High and Low Accelerations". J. of Spacecraft and Rockets, Vol 3, No. 12, December 1966.
9. L. L. Dachs: "Handling Liquid Propellants". Space/Aeronautics, October 1966.
10. R. T. Parmley: Phase I Final Report, In-Space Propellant Orientation and Venting Experiments. AFRPL-TR-66-270. Lockheed Missiles & Space Company, 31 October 1966.
11. M. P. Hollister, et al: A Study of Liquid Propellant Behavior During Periods of Varying Accelerations, Final Report. Contract NAS9-5174. IMSC-A874728, Code Y-87-67-1, Lockheed Missiles & Space Company, 30 June 1967.

12. H. R. Lundeen: Subcritical Liquid Oxygen Storage and Supply System For Use in Weightless Environments. Contract AF 33(615)-2308. AMRL-TR-66-178, The Bendix Corporation, Pioneer-Central Division, April 1967.
13. H. L. Paynter, et al: Final Design Report: Development of a Capillary System for Liquid Propellant Orientation During Low-G. TM-0444-66-3, Martin Marietta, Denver Division, Denver, Colorado, December 1965.
14. T. R. Barksdale and D. L. Balzer: Liquid Outflow Tests of Surface Tension Systems Under Minus One-G. TM-1661-66-12, Martin Marietta, Denver Division, Denver, Colorado, December 1966.
15. D. L. Balzer, et al: Capillary Systems For Storable Propellants. Section Report 1660-67-8. Martin Marietta, Denver Division, Denver, Colorado, June 1967.
16. J. C. Howell, et al: Main Tank Injection For Packaged Liquid Missiles, Phase I Report, Vol I - Systems Analysis and Component Tests. Contract AF 04(611)-11398. AFRPL-TR-66-115, Martin Marietta, Denver Division, June 1966. (Confidential)
17. M. P. Hollister: Propellant Containment Utilizing Screen Mesh and Perforated Plate Surfaces. LMSC-A665481, Code 9999, Lockheed Missiles & Space Company, 29 December 1964.
18. V. C. Oltrogge: Test Report, Bubble Retention Test - 624A. Martin Marietta, Denver Division, Denver, Colorado, 31 October 1963.
19. W. J. Masica, et al: Hydrostatic Stability of the Liquid-Vapor Interface in a Gravitational Field. NASA TN D-2267, May 1964.
20. Studies of Interfacial Surface Energies, Summary Report. Contract NAS3-5744, Report No. NASA CR-54175, Harris Research Laboratories, December 1964.
21. W. A. Zisman: "Relation of Equilibrium Contact Angle to Liquid and Solid Constitution". Contact Angle-Wettability and Adhesion, Adv. in Chem. Series No. 43, American Chemical Society, Washington, D.C., 1964, p. 20.
22. Study of Earth-Orbital Experiments For Low-Gravity Fluid Mechanics, Report No. P-66-51 (Vol. I), Martin Marietta, Denver Division, Denver, Colorado, June 1966, p. II-6.
23. D. E. Gilmore and T. R. Barksdale: Low-g Laboratory Annual Progress Report: 1965. Report No. TM-0444-66-2, Martin Marietta, Denver Division, Denver, Colorado, December 1965.

24. S. J. Kline and F. A. McClintock: "Describing Uncertainties in Single-Sample Experiments". Mechanical Engineering, January 1953.
25. J. J. Bikerman: Surface Chemistry. Academic Press, Inc., New York, 1958.
26. A. S. Povitskii and L. Ya. Lyubin: "The Outflow of Gas Into a Liquid Under Weightless Conditions". Cosmic Research, Vol. 3, No. 5, September-October, 1965.
27. P. G. Bhuta and L. R. Koval: Sloshing of a Liquid in a Draining or Filling Tank Under Variable G Conditions. Paper presented at Symposium on Fluid Mechanics and Heat Transfer Under Low Gravitational Conditions, Palo Alto, California, 24 and 25 June 1965.
28. Private Communication. L. J. Hastings, MSFC, and H. L. Paynter, MMC, 6 October 1967.

DISTRIBUTION

<u>Copies</u>	<u>To</u>
1 thru 15 plus one reproducible	Director George C. Marshall Space Flight Center National Aeronautics and Space Administration Huntsville, Alabama 35812 Attn: PR-RC
16 thru 50	Martin Marietta Corporation Denver Division Denver, Colorado

Appendix A: Literature Review

A survey of the literature pertaining to hydrostatic stability made by Dr. T. E. Bowman is presented as background material to this experimental study.

Perhaps the most logical starting point in any consideration of liquid-vapor interfaces is the question of static equilibrium shape of the interface. The monumental book in this area is that by Bashforth and Adams (Ref 1), who developed a method for numerically solving the equation of capillarity and presented the results in voluminous tables as a function of fluid properties, gravitational acceleration, and contact angle. They also presented a thorough survey of the capillarity literature up to the time of their work, and reported on some of their own experimental work that gave results in very good agreement with their numerical calculations. Fordham (Ref 2) has interpolated more detail into the Bashforth and Adams tables.

Bashforth and Adams confined their investigation to the case where the surface is symmetric about an axis parallel to the direction of the gravitational acceleration, arbitrary in magnitude but not direction. Works by Larkin (Ref 3 and 4) develop a method of solution for the more general problem of nonaxisymmetric surfaces and gravitational accelerations that are arbitrary in both direction and magnitude. Solutions are presented and agreement with the special case documented by Bashforth and Adams is shown. Two other works are also of interest. Journey (Ref 5) has adapted the tables of Bashforth and Adams to give interface shapes for known amounts of liquid contained in axisymmetric containers of various shapes (gravity, of course, being arbitrary in magnitude but not direction since the Bashforth and Adams tables were used). Satterlee and Chin (Ref 6) presented the results of a computer program for the description of the liquid/vapor interface in a right circular cylinder, axis parallel to gravity, which is perhaps more convenient to use than the Bashforth and Adams tables although it does not consider the more general problems investigated by Larkin or Journey.

Once the means of determining the shape of the liquid/vapor interface is understood, the next step toward arriving at a good theoretical understanding of foraminous material consists of analyzing the stability of the interface. Although Duprez (Ref 7) had studied the problem experimentally at an earlier date, the first formal analysis of stability of the interface between two fluids of different density was presented by Maxwell in his classical Encyclopedia Britannica

article on Capillary Action (Ref 8). Assuming a 90-degree contact angle, Maxwell considered the stability of the interface in orifices or tubes of both circular and rectangular cross section. In the case where the heavier fluid is on top of the lighter one, as in this experimental program, Maxwell's results can be manipulated to give a critical Bond Number* of 14.68 for a circular orifice, 12.35 for a square orifice, and 2.47 in the limiting case where the rectangular orifice becomes a two-dimensional channel of unlimited length. It should be pointed out that Maxwell's analysis employed linearized equations and he assumed that the location of the solid/liquid/vapor intersection was fixed. The linearization can be shown to lead to identically correct stability criteria in the special case of a 90-degree contact angle, although it might have little value for contact angles less than about 45 degrees. The second assumption is probably a good one in the case of foraminous material, although it may not be realistic in the case of interfaces located in tubes.

In the latter case, the only effect of this assumption is to forbid nonsymmetric solutions to the equations. Thus, in the circular case, Maxwell's results of 14.68 is always the correct stability criterion for the lowest axisymmetric mode. If Maxwell's analysis is extended to consider the nonsymmetric modes, it is found that the fundamental mode in the circular case becomes unstable at a Bond number of 3.39--the same result found by Satterlee and Reynolds (Ref 9) for the case of a 90-degree contact angle. The method of solution presented by Satterlee and Reynolds for this special case is, therefore, similar to Maxwell's method of solution without the assumption of axial symmetry. Maxwell's assumption of a stuck edge condition does not affect his result in the case of the channel, where there can be no corresponding symmetry considerations because of the two-dimensionality of the interface. Therefore, his result is the same as that found by Concus (Ref 10) for the 90-degree case.

It is an unfortunate result of the conciseness of Maxwell's presentation that his solution for the channel case is commonly attributed to Lamb (Ref 11), who himself apparently thought Maxwell had only considered cylinders (Ref 11, p. 461).

With the advent of digital computers, modern investigators are not restricted to the linearized analysis employed by Maxwell, and hence have been able to investigate the stability of interfaces with other than 90-degree contact angles. Perhaps the first of these more recent studies was made by Bretherton (Ref 13) who was interested in the maximum size of a stable interface with a zero contact angle.

*Bond number is based upon radius of the circular orifice or the half-width of the channel or square orifice.

Using a computer to investigate the equation of capillarity, he found that a Bond number of 0.842 corresponded to the largest possible equilibrium interface. As Bretherton pointed out, this value could have been obtained from the Bashforth and Adams tables, although the accuracy would not have been as great. While Bretherton did not actually concern himself with the question of the stability of the interface, but rather with the question of the existence of a solution to the capillarity equation, it has since been shown that the two criteria give the same result in the case of zero contact angle (Ref 9). This is in contrast to the previously discussed case of the 90-degree contact angle, in which the criterion of the existence of a solution to the capillarity equation places no limitation on the extent of the surface, and the only question of interest concerns the surface's stability. Although Bretherton apparently was not aware of the fact, his result of 0.842 for the critical Bond number was in very good agreement with earlier experimental findings by Hattori (Ref 13). The result has also been confirmed by more recent experimental work by Masica, et al, (Ref 14 and 15).

Probably the first investigation of interfacial stability in which contact angle was arbitrary, taking on any values, was by Concus (Ref 10), who considered the interfacial stability in an inverted, two-dimensional rectangular channel. He showed that the question of stability can be approached equivalently from minimum-energy considerations or from consideration of the eigenvalue problem associated with small perturbations of the interface from its equilibrium position. The latter approach is the one chosen by Maxwell and other classical investigators, while the former is more suitable for computer solution. Concus's results for critical Bond number increase monotonically with contact angle from 0.72 at zero (slightly less, as it should be, than Bretherton's value of 0.842 for the circular cylinder) to 2.47 at 90 degrees, in perfect agreement with Maxwell's result for the same case. As previously pointed out, for a two-dimensional channel, it makes no difference whether the solid/liquid/vapor intersection is assumed to be fixed or free to move.

Satterlee and Reynolds extended Concus's analysis to the case of vertical, circular cylinders, assuming arbitrary, constant contact angle and a free solid/liquid/vapor intersection (Ref 9). Their results for critical Bond number increased monotonically with contact angle from 0.825 at zero, in good agreement with Bretherton's result, to 3.39 at 90 degrees, the answer Maxwell would have gotten for this case had he relaxed his restriction of a fixed solid/liquid/vapor intersection. Maxwell required that the contact angle be 90 degrees. The only difference between Maxwell's analysis and that of Satterlee and Reynolds for the 90-degree case, as previously mentioned, is the fact that Maxwell fixed the position of his solid/liquid/vapor interface by discarding nonaxisymmetric solutions.

APPENDIX BIBLIOGRAPHY

1. F. Bashforth and J. C. Adams: An Attempt to Test the Theories of Capillary Action. University Press, Cambridge, England, 1883.
2. S. Fordham: "On the Calculation of Surface Tension from Measurements of Pendant Drops." Proceedings, Royal Society, Vol 194, 1948, p 1 thru 16.
3. B. K. Larkin: Numerical Solution to the Equation of Capillarity. Section Report 0560-65-3. Martin Company, Denver, Colorado, May 1965.
4. T. E. Bowman, B. K. Larkin and J. L. McGrew: Phase I Report, Criteria for Cryogenic Liquid Experiments in Orbit (CLEO). NASA-MSFC Contract NAS8-11328. Martin Company, Denver, Colorado.
5. W. H. Journey: The Configurations of Contained Liquids in Arbitrary Constant Gravitational Fields. TM 0444-65-4. Martin Company, Denver, Colorado, July 1965.
6. H. M. Satterlee and J. H. Chin: "Meniscus Shape Under Reduced-Gravity Conditions." Paper presented at Symposium in Fluid Mechanics and Heat Transfer Under Low-Gravitational Conditions, Palo Alto, California, 24 and 25 June 1965.
7. F. Dupres: "Sur un cas particulier de l' équilibre des liquides." Nouveaux Mém. de l' Acad. de Belgique, Vol. 26, 1851, and Vol 28, 1854.
8. J. C. Maxwell: "Capillary Action." The Scientific Papers of James Clark Maxwell, University Press, Cambridge, England, Vol 2, 1890, p 541 thru 591.
9. H. M. Satterlee and W. C. Reynolds: The Dynamics of the Free Liquid Surface in Cylindrical Containers Under Strong Capillary and Weak Gravity Conditions. TR No. LG-2. ME Department, Thermosciences Division, Stanford University, May 1964.
10. P. Concus: "Capillary Stability in an Inverted Rectangular Tank." Advances in the Astronautical Sciences, Vol 14, Western Periodicals Company, North Hollywood, California, 1963, p 21 thru 37.
11. H. Lamb: Hydrodynamics. Sixth Edition, University Press, Cambridge, England, 1932, and Dover Publications, New York, 1945.

12. F. P. Bretherton: "The Motion of Bubbles in Long Tubes." Journal of Fluid Mechanics, Vol 10, 1961, p 166 thru 188.
13. S. Hattori: On the Motion of a Cylindrical Bubble in a Tube and Its Application to the Measurement of the Surface Tension of a Liquid. Report N. 115. Aeronautical Research Institute, Tokyo Imperial University, 1935.
14. W. J. Masica, J. D. Derdul, and D. A. Petrash: Hydrostatic Stability of the Liquid/Vapor Interface in a Low-Acceleration Field. NASA TN D-2444, August 1964.
15. W. J. Masica, D. A. Petrash, and E. W. Otto: Hydrostatic Stability of the Liquid/Vapor Interface in a Gravitational Field. NASA TN D-2267, May 1964.